Designing an Innovative Brake Control System

EE3L11, Bachelor Thesis, July 12, 2017

Authors:	Bart Melman (4376684) Michael Treffers (4374614)
Supervisors:	dr. ir. H. Polinder ir. U. Shipurkar ir. R. Lenssen ir. S. Boersma
Jury:	dr.ir. I. Lager dr.ir. H. Polinder dr.ir. M. Ghaffarian Niasar

This thesis is confidential and cannot be made public

TU Delft Delft University of Technology

Abstract

Current trailers and caravans use overrun brakes, which cause overheated brakes in the mountains. A solution is to design an electric brake system in which the brakes are controlled electronically instead of mechanically. The report discusses the control models associated with braking, anti-sway detection and velocity sensor fusion. The RDW requires the force between the car and trailer to be regulated to zero within 0.6 seconds. The internal model based control method is used to design the controller. Test results show that the controller responds quick enough and is robust to disturbances. For the anti-sway detection, a calibration model is constructed that transforms the sensor data from the sensor's reference frame to the trailer's reference frame. Simulations with empirical data have verified the functionality of the calibration model. The angular yaw rate measured by a gyroscope can be used for anti-sway detection. A curve can be created that shows the relationship between the maximum allowed yaw rate and the velocity. In addition to that, an orientation model is constructed that can estimate the Euler angles and the gravity vector with a complementary filter. Consequently, the dynamic acceleration can be extracted obtained from the accelerometer. Several sensors are mounted to the E-Brake that can determine the velocity. A decentralised Kalman fusion filter is designed to estimate the velocity from the acceleration, velocity and GPS data.

Contents

1 Introduction

This thesis report is part of the final bachelor project in the third year of the bachelor Electrical Engineering at Delft University of Technology.

The introduction of the report is chapter 1. First, the context of the thesis subject will be explained and after that the three problem statements will be discussed. The state-of-the-art analysis section provides an overview of the existing control models in the industry and recent research studies that can be used for the design of new algorithms. Chapter 2 contains the requirements of the entire system. These come from patents, the RDW and the company E-Trailer. Chapter 3 contains the design process and justifications for the three different problem statements. Each problem statement is discussed in a separate section. Chapter 4 contains the test results from the different problem statements. The final three chapters are the discussion, conclusion and recommendation that are especially useful for groups that continue with the project.

1.1 Context

The thesis subject is submitted by the company E-Trailer, a startup at the incubator Yes!Delft. Their aim is to modernise the trailer and caravan industry by designing smart electronic systems. One of their new innovations is the E-Brake, an innovative electric brake system for trailers and caravans. Currently, caravans and trailers use an overrun brake, which is a spring in the hitch connection that pulls a brake cable if the spring is compressed. An overrun brake has several negative features that an electric brake can solve. First, moving downhill in the mountains causes the spring at the hitch connection to be compressed continuously. As a result, the brakes can become overheated. The algorithm of the E-Brake will solve this problem.

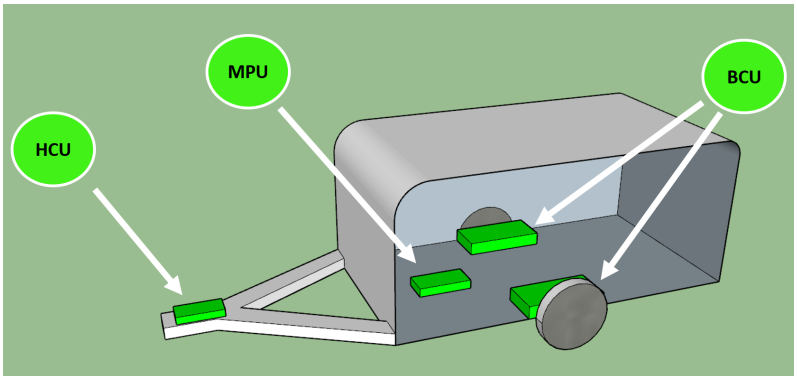

Figure 1: system decomposition

Secondly, current anti-swaying solutions brake both wheels of the trailer, thereby reducing the speed. The E-Brake can separately brake the wheels. As a result, the swaying is stopped without much reduction of the speed. The third problem for trailer users today is that the spring at

the hitch connection is compressed if the driver drives in reverse. The trailer brakes, making it impossible for the driver to drive in reverse. The electric brake system can detect reverse driving and does not brake in reverse driving mode.

The E-Brake consists of three different modules: the main processing unit(MPU), the hitch connection unit (HCU) and two brake control units (BCU). The modules are connected to a a CAN bus for communication. There is a single cable that provides the CAN bus connection and the power supply. The hitch connection unit measures the force between the car and the caravan with a load cell. The brake control unit controls the current flow through the brakes for a certain brake force and the main processing unit determines the brake force of the trailer with the load cell force of the hitch connection unit. The system decomposition is shown in figure 1. The thesis will focus on the algorithms and control of the main processing unit.

1.2 Problem Definition

The E-Brake has the capability to solve different problems for the consumer. The first task is straight forward: regulating the brake force, so that the trailer or caravan can brake on a horizontal road, in the mountains and during turns. Due to the limiting test time, the decision is made to limit the problem definition to a horizontal road.

Problem Statement 1:
Regulate the brake force of the trailer in accordance with the regulations of the RDW on a horizontal road during deceleration

The second task is sway detection to alert the consumer. The main processing unit contains a Bluetooth module that can communicate with a smartphone. There is no clear road to identifying swaying. Therefore the problem statement will be identifying the sensors and methods that can be used to design an algorithm.

Problem Statement 2:
Identify the sensors and methods needed for sway detection.

The velocity is a key factor for both the sway detection and the brake control group. The maximum allowed swaying is related to the velocity. At high speeds, high frequency swaying can quickly result in instability and an accident. At low velocities, higher frequency swaying is allowed. It can be compared with turning a car. At a highway it is difficult to make a quick turn, whereas at low velocities, turnarounds are no problem. The velocity is also used by the brake control group. The brake force is related to the velocity of the car trailer combination. The final problem statement is to identify the best way to combine multiple sensors, such as an accelerometer, GPS and a tachometer to optimally estimate the velocity.

Problem Statement 3:
Identify the qualities of the sensors to design a sensor fusion algorithm.

1.3 State-of-the-Art Analysis

The literature study has provided insight in the state-of-the-art systems and algorithms that are used for this or similar products. In the United States, an electric brake system is present that is manually controlled by the driver. If the driver wants to brake, then he moves a slider upwards and the brake force will be proportional to the acceleration measured by an accelerometer. It is bound by less regulations, since it is only an aid. Besides the brake system in the United States, there is no research done regarding problem statement 1. Regarding problem statement 2, there is already research done regarding swaying. Figure 2 shows the result of research[1] that shows the maximum safe yaw rate of the trailer versus the velocity of the trailer. It is a patent that has

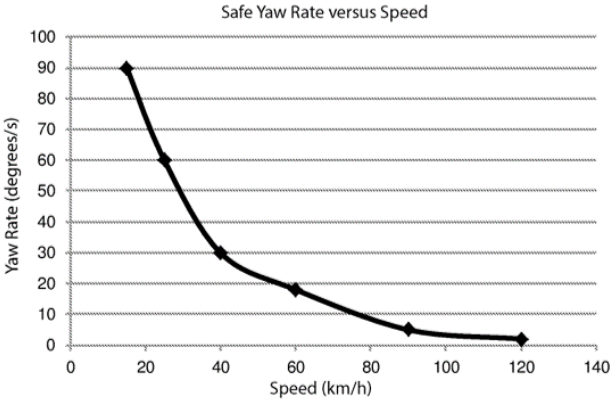

Figure 2: yaw rate versus velocity[1]

not been approved yet, but gives insight in the possibilities for sway detection.

The main processing unit can be mounted in any direction in the caravan. Therefore it is impossible to know the orientation of the trailer from the sensor data. A rotation matrix has to be constructed that rotates the sensor data to the trailer reference frame. After that, an orientation model has to be constructed that combines both acceleration data and gyroscope data to obtain the correct Euler angles[2]. Euler angles represent the orientation with respect to earth. One of the method is to use quaternions that avoid gimbal lock[3]. However, it depends on the way the algorithm is implemented, whether there are gimbal lock problems. There are roughly three methods of implementing a sensor fusion algorithm. The first implementation is a complementary filter that uses the accelerometer for the long term estimation of the gravity vector and the gyroscope for the short term changes in Euler angles. The second approach is to use a PID controller and the third approach is to use a Kalman filter[4]. The idea that the accelerometer is the long term predictor and that the gyroscope is the short term predictor is the same for all models, but the implementation is different.

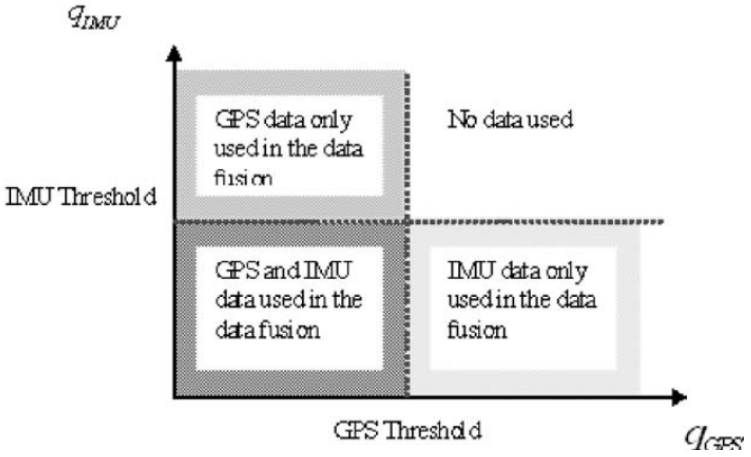

Figure 3: IMU and GPS fusion algorithm

For problem statement 3, research has been done on implementing a sensor fusion algorithm for the GPS and IMU (inertial measurement unit) for position estimation[5]. The IMU consists of a gyroscope and an accelerometer. The position is obtained by integrating the acceleration twice. A Kalman fusion algorithm combines both data to a single output based on the contextual

variables q_{IMU} and q_{GPS}. The contextual variables give an indication of the "trustworthiness" of the sensor output. A sensor output with a high value of q will have less impact on the new estimate than a sensor output with a low value of q. Figure 3, shows the effect of the contextual variable q to the validity of the sensor.

1.4 Thesis Synopsis

Currently trailers and caravans use overrun brakes, which can cause overheated brakes in the mountains. A solution to that problem is to design an electric brake system in which the brakes are controlled electronically instead of mechanically. A solenoid is placed at the wheel, which brakes the wheel if a current runs through it. The report answers the question: How to design an innovative braking control system? There are three control models designed that will be discussed seperately.

First, a control model is designed that brakes the trailer on a horizontal road according to the RDW regulations. The force between the car and the trailer is measured with a load cell at the hitch connection and needs to be regulated to zero, such that the trailer brakes itself. The internal model based approach is used to design the feedback loop. The output of the model is a reference brake force that is send to a brake control unit. The brake force is converted to a reference current. The report also discusses the current controller that regulates the current through solenoid to the reference value. An I-controller is used for the current controller, because the closed loop transfer will then be one pole with a cutoff frequency of $1\backslash$ I.

Secondly, an algorithm is constructed to detect swaying. The allowed angular velocity depends on the velocity of the trailer. In order to detect swaying, an accelerometer, a gyroscope and a velocity sensor are needed. If the angular yaw rate is higher than a threshold as a function of velocity, then the swaying is detected. The accelerometer is used for a calibration model that transforms the acceleration and angular velocity data from the sensor's reference frame to the trailer's reference frame. Also, an orientation model is constructed to remove the gravity vector from the data from the accelerometer to obtain the dynamic acceleration of the trailer. A complementary filter is used in the orientation mode to estimate the Euler angles. The gyroscope will predict the short term change in Euler angles and the accelerometer will be used as a long term predictor of the Euler angles.

Thirdly, a sensor fusion algorithm is explained that combines the data from the GPS, velocity sensor and accelerometer to more accurately estimate the velocity. A decentralised Kalman filter is used that allows sensors to temporarily become unreliable without the algorithm becoming unstable. The GPS is an accurate velocity sensor, but in tunnels the signal becomes unreliable. The decentralised Kalman filter is therefore suited for the problem.

Several tests have been carried out to test the orientation model and the hitch force control model. The sensor fusion model could not be tested, because the GPS module was not finished by the company E-Trailer in time. The orientation model was verified by driving up and down the hill of Delft Zuid. The conclusion is that the change of the yaw angle is clearly visible at the gyroscope, but that the change of the pitch and roll angle is not. The calibration model works accurately and allows the sensors to be mounted in any direction. The yaw rate, as well as the centripetal force are clearly visible in the sensor data. Both can be used as a measure of the sway rate of the trailer. Due to safety and limited time, no data was collected of the trailer swaying. The brake control model was verified by braking slowly and observing the load cell force. Unfortunately the brakes itself were not capable of braking with a large force. Therefore the force of the controller was sometimes higher than what the solenoid could take. Therefore tests were carried out during which the car only decelerated slowly. That data clearly showed that the control model regulated the load cell force to zero. The conclusion is that the controller functions properly.

2

Requirements

2.1 Introduction

The E-Brake is a safety-critical system, which makes the requirements essential for the design process. Both the absence of braking as too much braking force can result in serious accidents. The main goal of the requirements is to create a framework of boundary conditions that allow the rarest situations to occur. For certain design requirements, safety factors are introduced to cover rare situations. The requirements for the main processing unit come from three sources: patents, the RDW (Rijksdienst voor het Wegverkeer) and E-Trailer. Firstly, research has already been done on electric brakes. Issued patents by other companies forbid certain control methods to be used in the E-Brake. In section 2.2 the implications of the patent system are discussed. Secondly, the RDW has specified different regulations for the approval of the system. In section 2.3, the process of approval is discussed. In section 2.4, further requirements by E-Trailer are presented and motivated. Once the system is approved, the liability still remains at the company. Therefore, it is in the company's interest to create a safe system and provide further requirements.

2.2 Patent Analysis

The E-brake is a new innovative product that will first be introduced by E-Trailer in the caravan market. Therefore it is important to know if the use of certain sensors or techniques is forbidden and for what period. E-Trailer has done thorough research on international patents regarding electric braking systems using a hitch connection. The results and implications are discussed next.

The most important existing patent is "US 20050006952 A1"[6]. In this patent, the method for electric braking of trailers using a load cell is claimed. The patent is granted to different countries, like the Netherlands, Germany, France and Great Britain. Most of these patents have expired, except for the ones in Germany [7] and the United States [6]. The patent in Germany expires at most in 2022.

The system is expected to be introduced on the market in the Netherlands in 2019. The E-brake will not be launched in all countries at ones. Year by year, the product will be introduced in another countries. First, the countries without an expired will be target. That will take several years. After that, all patents will have expired and the product can be launched in the United States and Germany.

2.3 RDW Regulations

The RDW (Rijksdienst voor het Wegverkeer) is a governmental organisation responsible for the regulation of the trailers and caravans in the Netherlands. The RDW has published the test procedure used to test and approve the electric braking system[8]. The most relevant regulations are split into two groups: communication and braking. The communication regulations discuss how the system should respond in case of failure during transmission. The braking regulations

discuss how much the trailer should brake and how it is measured in the test phase.

Communication regulations:

- 5.1.1.5 data failure
  - "A failure detection signal may interrupt momentarily (<10 ms) the demand signal in the control transmission, provided that the braking performance is thereby not reduced."
    The conclusion is that serial communication has to be used instead of a analog line signal to communicate between the brake control unit and the main processing unit.

Braking regulations:

- 1.1.2
  - "The mean fully developed deceleration (d_m) shall be calculated as the deceleration averaged with respect to distance over the interval v_b to v_e, according to the following formula":
    $$d_m = \frac{V_b^2 - V_e^2}{2 * (s_e - s_b)} \tag{1}$$
    Where:
    v_o = initial vehicle speed in m/s,
    v_b = vehicle speed at 0.8 v_o in m/s,
    v_e = vehicle speed at 0.1 v_o in m/s,
    s_b = distance travelled between v_o and v_b in metres,
    s_e = distance travelled between v_o and v_e in metres.
    The conclusion is that during the test days, start and end velocities need to be measured, as well as the start position and stopping position.

The mean fully developed deceleration can be derived by starting to equal the difference of kinetic energy to the integral of the force with respect to the distance.

$$\Delta E_k = \int_{s_b}^{s_e} F_{brake} dx \tag{2}$$

$$\frac{1}{2} * m * (v_b^2 - v_e^2) = \int_{s_b}^{s_e} m * a dx \tag{3}$$

$$\frac{1}{2} * (v_b^2 - v_e^2) = \int_{s_b}^{s_e} a dx \tag{4}$$

If equation 4 is substituted into equation 1, then equation 5 is obtained. The deceleration can be interpreted as the averaged acceleration, not in time, but in distance domain. It can be measured by sampling the accelerometer every rotation of the wheel and then taking the average of all acceleration values.

$$d_m = \frac{\int_{s_b}^{s_e} a dx}{s_e - s_b} = \frac{\int_{s_b}^{s_e} a dx}{\int_{s_b}^{s_e} dx} \tag{5}$$

- 3.1
  - "Electrical braking systems shall respond at a deceleration of the tractor/trailer combination of not more than 0.4 m/s^2."
    The conclusion is that the acceleration can be used to determine if the control model complies with this regulation.

- 3.2
  - "The braking effect may commence with an initial braking force, which shall not be higher than 10 per cent of the (sum of the) maximum stationary axle load(s) nor higher than 13 per cent of the (sum of the) stationary axle load(s) of the unladen trailer."
    The conclusion is that the step of maximum braking force difference is limited. The rising slope of the controller should therefore be tuned, so that the rising slope is not too steep.
- 3.3
  - "The braking forces may also be increased in steps. At higher levels of the braking forces than those referred to in paragraph 3.2. Of this annex these steps shall not be higher than 6 per cent of the (sum of the) maximum stationary axle load(s) nor higher than 8 per cent of the (sum of the) stationary axle load(s) of the unladen trailer."
    The same conclusion holds as for regulation 3.2.
- 3.5
  - "The test shall be carried out with an initial speed of 60 km/h."
    The conclusion is that the start velocities at the first test days will also be at 60 km/h for the feasibility study.
- 4.1.1
  - The control system should respond within 0.6 seconds of an emergency manoeuvre.
    Regulation 4.1.1 puts a restriction on the control model of the main processing unit. The transfer between the braking force of the car to the load cell should have a rise time of 0.6 seconds.

The RDW requirements[8] contain figure 4 that shows the relationship between the mean to develop deceleration(d_m) on the horizontal axis and the braking force of the trailer ($F_{trailer\_brake}$) divided by the normal force($F_{normal\_trailer}$) on the vertical axis. The red line is the ideal braking line. The black lines are the boundary lines, within one needs to brake. The plot also contains the boundary for multi-axle trailers. Multi-axle trailers are outside the scope of the thesis, so that line can be neglected.

The "ideal" line of figure 4 is equation 6. If the mass of the trailer is brought to the right side, then equation 7 is obtained. The physical interpretation is that the trailer has to brake itself. The acceleration that a car reaches with a certain braking force without the trailer should be the same as with the trailer. The trailer therefore has to brake itself.

$$\frac{F_{brake\_trailer}}{m_{trailer} * g} \approx 1/10 * d_m \tag{6}$$

$$F_{brake\_trailer} \approx m_{trailer} * d_m \tag{7}$$

2.4 Further Requirements

The RDW has imposed same minimum level of regulations that the system has to comply with. However, there are more requirements needed in order to make a robust system. These requirements come partially from the company and partially from a technical point of view. These are the further requirements:

1. The system should be designed to brake a single axle caravan or trailer of maximally 1800 kg. The reason is that there are no caravans on the market with a higher mass;
2. The slope of the brake response should be limited to optimise the drive experience;

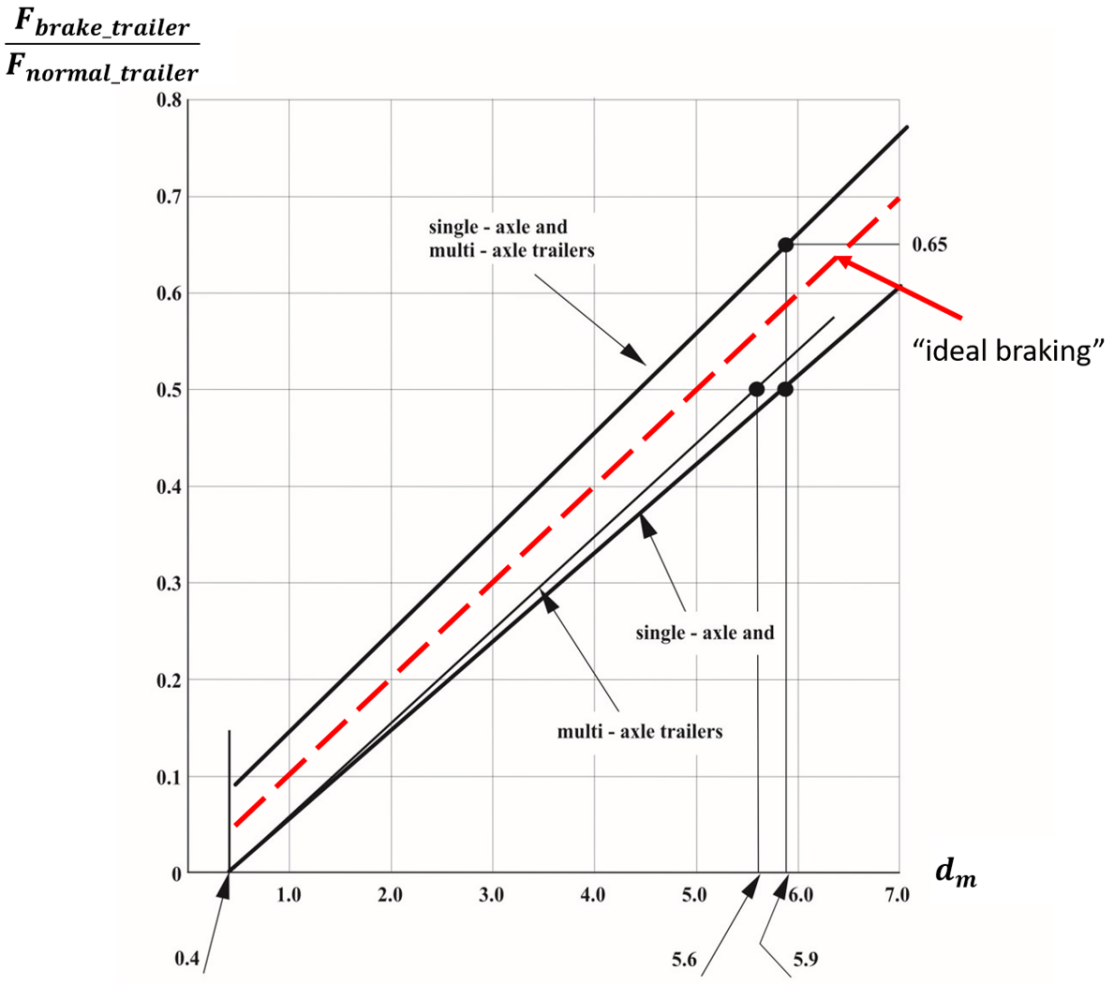

Figure 4: RDW required braking force[8]

3. The control algorithm should be robust and stable;
4. Error messages need to be send from the microcontroller in case of an error or a rare event;
5. The anti-sway algorithm needs to distinguish turning from swaying;
6. No infinite code loops need to be possible;
7. In case of a communication error during testing, send reference brake forces of zero(during testing only);

3

Design Process and Justifications

The requirements and the state-of-the-art analysis have been described in the previous chapters. This chapter contains the designs and simulations for the different problem statements. The main goal of the thesis is problem statement 1. The testing will be primarily focused on problem statement 1. For that problem, the digital implementation and variable values are provided. With the other problem statements, the focus is more on the design than the implementation.

3.1 Assumptions

In order to create effective solutions for the problem statements, several assumptions have to be made about the behaviour of the car trailer combination and the usage of it.

1. The mass of the trailer/caravan is maximally 1800 kg(the heaviest caravan is 1800 kg);
2. A single-axle trailer/caravan is used;
3. The steepest hill is 35 %;
4. The load cell is a rigid connection between the car and trailer;
5. The only resistive forces are roll resistance and air resistance;
6. There is no vertical force at the towbar;

3.2 Problem Statement 1: "Designing a Brake Control Algorithm"

The main goal of the thesis is problem statement 1: designing a brake control algorithm on a horizontal road. Firstly, a mechanical analysis is done of the car-trailer combination, containing free body diagrams and a resistive force decomposition. Secondly, a current control model has to be designed for the brake control unit. The current through the solenoid is measured by the brake control unit, but might not be equal to the reference current due to temperature effects. The current controller removes the steady state error between the measured current and the reference current. Thirdly, a control model has to be designed to brake the trailer according to the RDW regulations. The current control model parameters have an effect on the controller design of the hitch force control model. Therefore, the current control model is discussed first. Figure 5 shows the information flow of the sensors and how the control models relate to each other.

3.2.1 Mechanical Analysis

The mechanical analysis consists of two parts. In the first part, the free body diagrams are shown and explained. In the second part, equations are given that calculate the magnitude of the different forces.

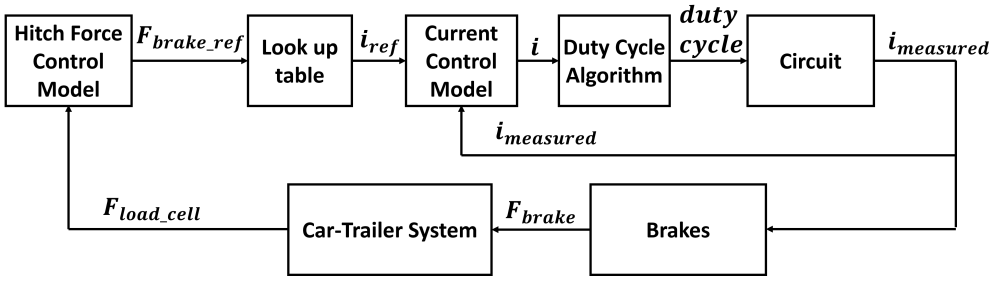

Figure 5: overview of hitch force control model and current control model

3.2.1.1 Free Body Diagrams

In order to characterise the mechanic behaviour of the vehicle trailer combination, several free body diagrams have to be constructed. Figure 6 shows the three free body diagrams, separated by two blue vertical dotted lines. The left free body diagram shows the forces that interact with the towing vehicle(car). The middle diagram shows the forces that interact with the load cell. The load cell is modelled as a rigid connection. That means that the forces on both sides are the same in magnitude, but in opposite direction. The right diagram shows the forces that interact with the trailer. The interpretation of the forces of the figure is shown in table 1.

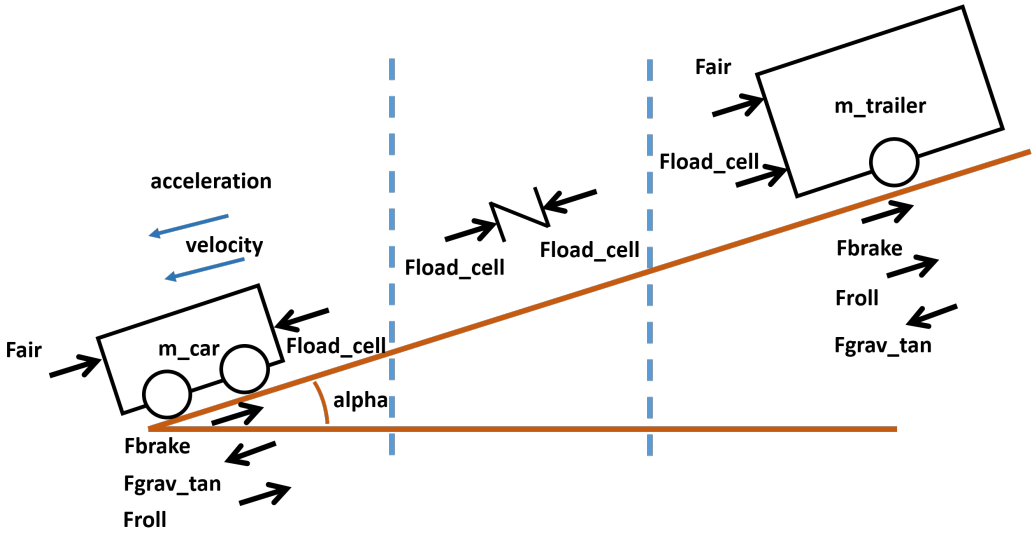

Figure 6: free body diagrams of (from left to right): car, load cell, trailer

Table 1: Force Abbreviations and Description

Abbreviation	Description
F_{brake}	braking force of the vehicle in the free body diagram
F_{load_cell}	force of load cell
F_{air}	air resistance of the vehicle in the free body diagram
F_{roll}	roll resistance of the vehicle in the free body diagram
F_{grav_tan}	tangential gravity force of the vehicle in the free body diagram

One approach is to model the load cell as a spring in parallel with a damper. If a force is applied, then the length of the material increases or decreases depending on the direction of the forces. However, due an extremely small distance difference, the connection can be assumed to be a rigid connection. The velocity and acceleration of the towing vehicle and the connected trailer are assumed to be the same.

In the design model, there are only two resistive forces: the roll resistance and the air resistance. There are two brake forces, the brake force of the car and the brake force of the trailer. The brake force is always defined as the sum of braking forces on all wheels of the vehicle. Equations 8 and 9 show the resultant forces of the car and trailer based on the free body diagrams of figure 6.

$$\begin{aligned} F_{car\_res} &= m_{car} * a \\ &= F_{load\_cell} - F_{car\_resistance\_air} - F_{car\_resistance\_roll} - F_{car\_brake} \\ &\quad + F_{car\_gravity\_tangential} \end{aligned} \tag{8}$$

$$\begin{aligned} F_{trailer\_res} &= m_{trailer} * a \\ &= -F_{load\_cell} - F_{trailer\_resistance\_air} - F_{trailer\_resistance\_roll} \\ &\quad - F_{trailer\_brake} + F_{trailer\_gravity\_tangential} \end{aligned} \tag{9}$$

The effect of the air resistance and roll resistance is interesting, but difficult or unable to predict. For example, with the current selection of sensors, the effect of wind cannot be included. In addition to that, the roll resistance is majorly dependent on the the pressure and the type of the tire. Problem statement 1 can be further specified. The sum of the resistive forces and brake force of the trailer should make the load cell force zero.

Algorithm Goal:
The goal of the algorithm is to regulate the brake force of the trailer such that the force measured at the load cell is zero.

3.2.1.2 Force Analysis

In the existing test configuration, it is not possible to measure the roll and air resistance. However, there are several relationships that estimate the magnitude of these forces. These formula's can be used during the design phase to observe the effect of transient behaviour on these resistances.

The rolling resistance can be computed with equation 10 [9]. The rolling resistance coefficient c depends on the velocity and the tire pressure. As the pressure increases, the rolling resistance decreases and as the velocity increases, the rolling resistance increases. However, due to the fact that there can also be a lot of other road types, the coefficient is assumed to be constant for the simplicity of the model. The coefficient ranges between 0.01 and 0.03.

$$F_{roll} = c * g * m \tag{10}$$

The drag equation (equation 11) shows the relationship between the air resistance, velocity, cross section area, density and the drag coefficient. This equation can be used to derive the air resistance of the car and the trailer.

$$F_{air} = \frac{1}{2} * \rho * v^2 * C_w * A \tag{11}$$

The drag coefficient C_w of a car varies from 0.25 to 0.45 for a SUV[10]. The frontal area can range from 2 to 4.6 m^2 [11].

$$F_{car\_resistance\_air} = \frac{1}{2} * \rho * v^2 * C_{w\_car} * A_{car} \tag{12}$$

The drag coefficient of a trailer is approximately 0.5 for a "streamlined" caravan. That means that the edges are not oblique, but rounded. The most resistive caravan has a drag coefficient of 0.67[12].

$$\begin{aligned} F_{trailer\_resistance\_air} &= \frac{1}{2} * \rho * v^2 * C_{w\_trailer} * A_{trailer\_eff} \\ &= \frac{1}{2} * \rho * v^2 * C_{w\_trailer} * (A_{trailer} - A_{car}) \end{aligned} \tag{13}$$

The drag force is quadratically dependent on the air velocity. Especially at high velocities, the effect of deceleration on the drag force has to be taken into consideration. The difficulty is that the frontal area of the trailer and car vary a lot, which makes it harder to implement in a controller. The final force that impacts the car-trailer combination is the tangential force of the gravity. The tangential component of the gravity vector depends on the slope angle α.

$$F_{car\_gravity\_tangential} = m_{car} * g * sin(\alpha) \tag{14}$$

$$F_{trailer\_gravity\_tangential} = m_{trailer} * g * sin(\alpha) \tag{15}$$

3.2.2 Current Control Model

Due to the temperature of the solenoid, the reference current is not equal to the output current. Therefore, the current through the solenoid has to be regulated. A current sensor measures the actual current through the solenoid. The solution is to design a feedback loop that makes the steady state error zero. The closed loop characteristics will be incorporated in the hitch force control model. Therefore, there are also requirements from the hitch force control model.

3.2.2.1 Feedback Loop

The designed current feedback loop in figure 7 consists of several blocks, which will be discussed one by one. The brake control unit (BCU) receives a force from the main processing unit (MPU) and converts that with a LUT(lookup table) to a reference current. The actual current is the output of the feedback loop. There is a noise source N(s) caused by the current sensor. C(s) is the transfer function of the controller and the transfer function of the plant is represented with G(s). The transfer function of the plant is discussed in section 3.2.2.3. Pulse width modulation(PWM) will be used to control the current through the solenoid. The PWM signal cannot have a duty cycle higher than 100 %. Therefore, there is a saturation block between the controller and the plant to specify the maximum current that can be reached with a duty cycle of 100 %. One of the properties of a feedback loop is that there can be overshoot. At high reference currents, that could mean that the output current of the controller is saturated. As a result, the model becomes nonlinear. This has to be taken into consideration in the controller design. The control has to be designed such that the saturation reference brake force is not reached with the maximum overshoot.

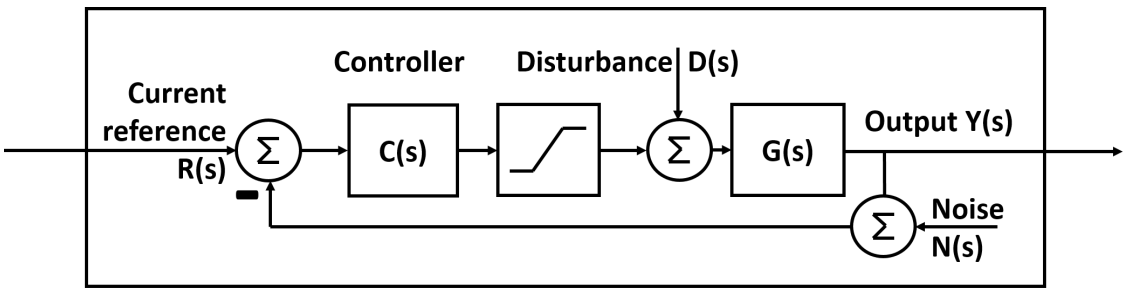

Figure 7: current control feedback loop

3.2.2.2 Requirements

The current control model has requirements based on the hitch force control model and the properties of the solenoid. Temperature influences the resistance and inductance of the solenoid. Instead of designing an optimal controller, robust control will be used to ensure stability.

1. The bandwidth of the closed loop transfer function should be lower than half the sampling frequency of the hitch control model or at least a factor 2 higher;
2. The steady state transfer of disturbances should be zero;
3. Overshoot must be avoided;
4. The poles in the s-domain must be located in the left-half plane and the poles in the z-domain must be located in the right-half plane;
5. The controller should be stable for all possible resistance and inductance values of the solenoid;
6. The phase margin(PM) must be higher than 30 °;
7. The gain margin must be bigger than 5 for the worst case scenario solenoid;
8. High frequency noise should be suppressed as much as possible;

3.2.2.3 Model of the Solenoid

In order to design the controller C(s), the transfer function of the plant has to be known. The plant is the transfer of a non-ideal inductor. A non-ideal inductor is a resistor in series with an ideal inductor. The relationship between the reference current and the measured current is shown in equation 16.

$$G(s) = \frac{i_{measured}(s)}{i_{ref}(s)} = \frac{R}{R + L * s} \tag{16}$$

The transfer of the plant of the current control model is equation 16. The resistance and inductance of the solenoid vary with temperature. The first step is to identify the range of values that the resistance and inductance can take. The brake control group came with the following test results:

Table 2: empirical temperature inductance relation

Temperature [°C]	**Inductance [mH]**
23	8.6
36	9.1
60	9.3
140	9.7

Table 3: empirical temperature resistance relation

Temperature [° C]	**Resistance [Ω]**
24	3.084
30	3.68
40	4.19
50	4.87
60	5.18
70	5.91
90	7.08

Several conclusions can be drawn from the test results. Firstly, the resistance and inductance increase monotonic with the temperature within the measurement range. Secondly, the inductance

can be assumed to be within 8.6 mH and 9.7 mH and the resistance is situated between 3.084 Ω and 7.08 Ω. The pole of the plant is situated at -$\frac{R}{L}$ and ranges between -250 and -875. The time constant is $\frac{L}{R}$, which is in the order of milliseconds, which is less than the sample frequency.

3.2.2.4 Controller Design

As explained in the requirements section 3.2.2.3, the goal of the controller is not to decrease the rise time of the current through the inductor, but to reduce the steady state error to zero as fast as possible without overshoot. There are several blocks that can result in a gain error, so the gain margin has to be higher than 5. The model will be validated by considering the following two cases:

1. the plant has R and L values for the smallest pole
2. the plant has R and L values for the largest pole

The following transfer functions demonstrate the relationships of the reference R(s), disturbance D(s), noise N(s) and output Y(s):

$$\frac{Y(s)}{R(s)} = \frac{C(s) * G(s)}{1 + C(s) * G(s)} \tag{17}$$

$$\frac{Y(s)}{D(s)} = \frac{G(s)}{1 + C(s) * G(s)} \tag{18}$$

$$\frac{Y(s)}{N(s)} = -\frac{C(s) * G(s)}{1 + C(s) * G(s)} \tag{19}$$

$$\frac{E(s)}{R(s)} = \frac{1}{1 + C(s) * G(s)} \tag{20}$$

As can be seen from equation 17 and 19, the noise cannot be reduced in the system's operating frequency band, because both transfer functions are the same. The transfer functions of equation 18 and 20 are the same. Both equations are designed to have a steady state error of zero.

The plant will be modelled as 1 for the controller design, since the pole of the solenoid is larger than the sample frequency. Initially, a PI controller is designed instead of a PID controller, because the D part is difficult to implement in the digital domain. Noise makes it difficult to take the derivative of a signal. The following transfer functions are the result:

$$C(s) = P + \frac{I}{s} \tag{21}$$

$$\begin{aligned} \frac{Y(s)}{R(s)} &= \frac{P + \frac{I}{s}}{1 + P + \frac{I}{s}} \\ &= \frac{I + P * s}{I + (1 + P) * s} \end{aligned} \tag{22}$$

If P is chosen as 0, then the closed loop transfer reduces to:

$$\frac{Y(s)}{R(s)} = \frac{I}{I + s} \tag{23}$$

The advantage is that the closed loop transfer becomes a first order system that can easily be used by the hitch control model. In addition to that, there is only one parameter I that needs to be chosen. The other transfer functions are:

$$\frac{E(s)}{R(s)} = \frac{Y(s)}{D(s)} = \frac{s}{s+I} = 1 - \frac{I}{s+I} \tag{24}$$

$$\frac{Y(s)}{N(s)} = -\frac{I}{I+s} \tag{25}$$

As can be seen in the previous transfer functions, the steady state error compared to a constant reference is zero and high frequency noise is rejected. The integrator coefficient I has to be chosen such that enough noise is suppressed, but that the closed loop response is still quick enough. The angular sampling frequency should be at least 10 times the closed loop bandwidth[13].

$$\omega_s \geq 10 * I \tag{26}$$

The rise time (0 % to 90 %) of the first order closed loop transfer is:

$$t_r = \frac{2.3}{I} \tag{27}$$

3.2.2.5 Simulation Results

The sample frequency of the current sensor is 200 Hz. Therefore, the maximum value of I is 120. The sample frequency of the hitch force control model is 80 Hz. An I of 30 is chosen. Then, the current control model responds quickly enough to the temperature effects, while leaving enough bandwidth for the hitch force control model. The closed loop current transfer has a pole lower than half the sample frequency of the hitch force control model, which is a requirement. Table 4 shows the properties of the controller with the extreme case plants.

Table 4: current controller parameters

pole position	**rise time $\frac{Y(S)}{R(s)}$ [s]**	**phase margin [°]**	**gain margin**
pole at -250 (maximum)	0.0645	83	inf
pole at -875 (minimum)	0.0707	88	inf

The worst and best case rise times differ with approximately 10 %. That situation is accepted. The phase margin is 90 %, which is much better than the specified 30%. The gain margin is infinite. It can be concluded that the I controller functions as a robust control model. Figure 8 shows the bode plots for the open loop and closed loop characteristics of the controller with the minimum and maximum plant. The theoretical rise time is 0.0767. The actual rise time is maximally 16 $\%$ from the value. That is acceptable.

3.2.2.6 Digital Implementation

The controller design in the previous section has been done in the s-domain. In order to implement the controller on a chip, the controller transfer function has to be converted to the digital domain. The bilinear transform is used to transfer equation 29 to equation 30.

$$s = \frac{2}{T} * \frac{1-z^{-1}}{1+z^{-1}} \ : \ bilinear\ transform \tag{28}$$

The following equation is the controller transfer function in the s-domain:

$$C(s) = \frac{I}{s} \tag{29}$$

The following equation is the controller transfer function in the z-domain:

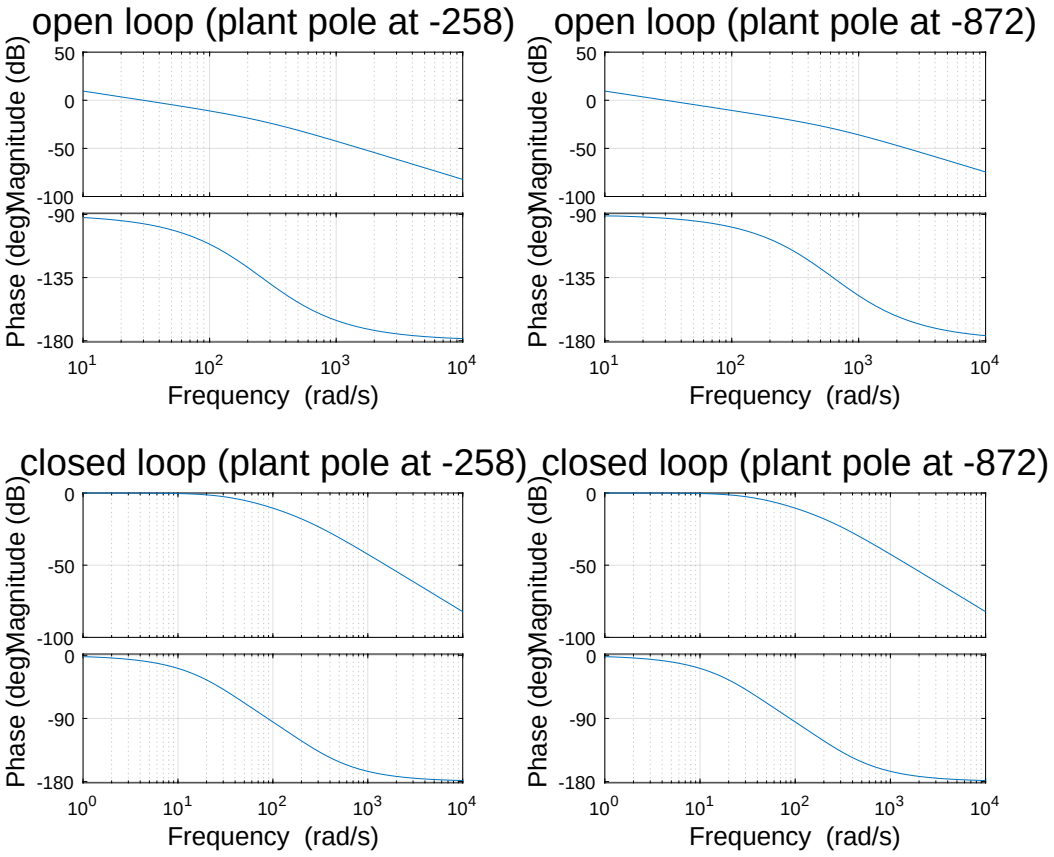

Figure 8: open loop and closed loop bode plots for the extreme poles of the solenoid

$$C(z) = \frac{I}{2 * f_s} * \frac{1 + z^{-1}}{1 - z^{-1}} \tag{30}$$

The pole of the transfer function is situated on the unit circle. That is expected, because an integrator is used. A saturation block is placed after the controller to limit the output current due to a maximum duty cycle of 100%. Therefore a concept is introduced called anti-windup. Once the output of the controller crosses the maximum current, the output is set at the threshold value.

3.2.3 Hitch Force Control Model

The main goal of the main processing unit is to regulate the brakes to make the force at the load cell zero. If the force measured at the load cell is zero, then the trailer brakes itself. The input of the model is the force measured at the load cell and the output of the model is a reference braking force for the brake control unit. First, a system decomposition will be done to characterise the relationship between the brake force and the load cell force. After that, the feedback loop will be discussed. The controller design will discus the design in s-domain and the digital implementation will transform the controller from the s-domain to the z-domain.

3.2.3.1 System Decomposition

In order to design the control loop, the ratio between a difference in the trailer's braking force and the force measured at the hitch connection has to be determined. An extra trailer braking force of 1 N does not result in 1 N less force at the load cell. The following equations will derive the relationship between the braking force and the force at the load cell. The direction of the forces are specified in figure 6.

The resultant force of the trailer is equal to the sum of all forces acting on the trailer (equation 32). The problem is that there can be no direct transfer from the load cell force to the brake force yet, since the acceleration is also dependent on the brake force of the trailer. Therefore the acceleration has to be expressed as a function of all forces on the trailer. That is done in equation 31. The next step is that the acceleration is substituted. The result is equation 33.

$$\begin{aligned} a &= \frac{F_{tot\_res}}{m_{tot}} \\ &= -\frac{F_{car\_brake} + F_{trailer\_brake} + F_{car\_air} + F_{trailer\_air} + F_{car\_roll} + F_{trailer\_roll} - F_{tot\_grav}}{m_{car} + m_{trailer}} \\ &= -\frac{F_{car\_brake} + F_{trailer\_brake}}{m_{car} + m_{trailer}} - \frac{F_{tot\_air}}{m_{car} + m_{trailer}} - c * g + sin(\alpha) * g \end{aligned} \tag{31}$$

$$\begin{aligned} F_{trailer\_res} &= m_{trailer} * a \\ &= -F_{load\_cell} - F_{brake\_trailer} - F_{trailer\_air} - F_{trailer\_roll} + F_{trailer\_grav} \end{aligned} \tag{32}$$

$$\begin{aligned} F_{trailer\_res} &= m_{trailer} * \Big(- \frac{F_{car\_brake} + F_{trailer\_brake}}{m_{car} + m_{trailer}} - \frac{F_{tot\_air}}{m_{car} + m_{trailer}} - c * g + sin(\alpha) * g \Big) \\ &= -F_{load\_cell} - F_{brake\_trailer} - F_{trailer\_air} - F_{trailer\_roll} + F_{trailer\_grav} \end{aligned} \tag{33}$$

The force on the load cell is now part of the equality without the acceleration being part of it as an explicit variable. Equation 34 has the force on the load cell as a function of the brake force with multiple disturbances. Disturbance $D(v^2)$ is the disturbance due to the air resistance and is dependent on the velocity squared. Disturbance $D(c)$ is caused by a difference in rolling coefficients of the tyres of the car and trailer.

$$\begin{aligned} F_{load\_cell} &= \frac{m_{trailer}}{m_{car} + m_{trailer}} * F_{car\_brake} - \frac{m_{car}}{m_{car} + m_{trailer}} * F_{trailer\_brake} \\ &\quad + \frac{m_{trailer}}{m_{car} + m_{trailer}} * F_{car\_air} - \frac{m_{car}}{m_{car} + m_{trailer}} * F_{trailer\_air} \\ &= -\frac{m_{car}}{m_{car} + m_{trailer}} * F_{trailer\_brake} + D(v^2) + D(c) + D(F_{car\_brake}) \\ &where: \\ &D(v^2) : disturbance\ of\ air\ resistance \\ &D(c) \ : constant\ disturbance\ due\ to\ roll\ resistance \\ &D(F_{car\_brake}) \ : disturbance\ due\ to\ the\ car\ braking \end{aligned} \tag{34}$$

In order to decide which brake force is required when the load cell measures a certain force, the following formula needs to be applied:

$$\Delta F_{trailer\_brake} = -F_{load\_cell} * \frac{m_{car} + m_{trailer}}{m_{car}} \tag{35}$$

Unfortunately, the masses of the of the car and the trailer are unknown.

$$1 \leq \frac{m_{car} + m_{trailer}}{m_{car}} \tag{36}$$

The mass of the car is at least 1200 and maximally 3000 kg. A caravan can be at least 150 and maximally 1800 kg. The algorithm will be designed for trailers and caravans. When the previously discussed constraints are added to equation 36, the following relationship holds:

$$1.08 \leq \frac{m_{car} + m_{trailer}}{m_{car}} \leq 2.5 \tag{37}$$

3.2.3.2 Feedback Loop

In this section, the feedback loop to regulate the force at the load cell is designed and explained. The feedback loop is shown in figure 9. The measured output of the feedback loop is the force at the hitch connection. A noise source N(s) is added to the load cell force to simulate the noise added by the load cell measurement unit. The force at the load cell is measured with strain gauges in a Wheatstone bridge configuration. Noise is added by the resistors in the Wheatstone bridge and by the AD converter. The noise source is band-limited due to the anti-aliasing filter. It can be assumed that the noise source is a Gaussian white noise source. The reference input is a load cell force of 0 N.

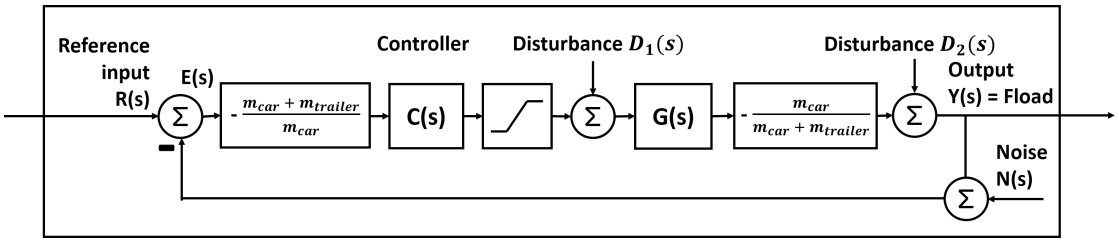

Figure 9: feedback loop of hitch force control model

The error is multiplied by a factor depending on the masses of the trailer and the car to determine the correct difference in brake force that should result in the force at the load cell to go to zero. The controller C(s) will initially be designed as a PI controller, because a D part is difficult in discrete time with noise. After the controller, there is a limiter, which maximises the output force send to the brake control unit. Physically, it is impossible for the brake control unit to brake higher than a certain force, since the duty cycle cannot be higher than 100 %. Therefore, it is useless to send a higher force than the saturation force.

The plant is the behaviour of the brake control unit. The transfer function of the brake control unit is G(s),the closed loop transfer function of the current control model. It is assumed that except for the current controller and the solenoid, there will be no delays or frequency dependent components in the conversion from current to brake force. The brake control unit uses a lookup table (LUT) to translate the required brake force to a reference current. Disturbance $D_1(s)$ is added to represent the errors from the lookup table. After the plant, the brake force is multiplied with a factor determined by the masses of the car and trailer to determine what effect the brake force has on the force measured at the load cell. The final disturbance is $D_2(s)$. Firstly, the braking force of the car is part of the disturbance. Secondly, the air resistance of the trailer relative to the car is a disturbance. The other components of disturbance D_2 are the air resistance and the roll resistance. The formula containing the decomposition of disturbance D_2 is shown in equation 34.

3.2.3.3 Requirements

The requirements for the hitch force control model are based on regulations of the RDW, the rejection of noise and disturbance sources and the saturation blocks that are included. The requirements are:

1. The steady state transfer of $\frac{Y(s)}{D_1(s)}$, $\frac{Y(s)}{D_2(s)}$ and $\frac{E(s)}{R(s)}$ is zero
2. The phase margin(PM) is larger than 30 °[14]
3. The poles of all transfer functions are situated in the left half plane
4. The rise time(t_{rise}) of $\frac{Y(s)}{R(s)}$ and $\frac{Y(s)}{D_2(s)}$ are smaller or equal to 0.6 (RDW requirement)
5. The overshoot of the braking reference force should be lower than 10 %
6. The gain margin(GM) should be high enough to counter variations in the plant and look up tables
7. Anti windup must be used in case the controller contains an I element
8. There should not be abrupt jumps in the braking force, because of the comfort of the system.

3.2.3.4 Controller Design

At this stage, all transfer function of the blocks in the feedback loop are known. Equation 38 shows the transfer function of the current controller G(s). It is assumed that the transfer function will not behave much different due to temperature differences of the solenoid, because the pole of the closed loop is much closer to the imaginary axis than the pole of the solenoid itself. A value for I of 30 is used.

$$G(s) = \frac{30}{s + 30} \tag{38}$$

The next equations show the transfer functions used in the controller design:

$$\frac{Y(s)}{R(s)} = \frac{C(s) * G(s)}{1 + C(s) * G(s)} \tag{39}$$

$$\begin{aligned} \frac{Y(s)}{D_1(s)} &= \frac{G(s)}{A * (1 + C(s) * G(s))} \\ with\ A &= -\frac{m_{car} + m_{trailer}}{m_{car}} \end{aligned} \tag{40}$$

$$\frac{Y(s)}{D_2(s)} = \frac{E(s)}{R(s)} = \frac{1}{1 + C(s) * G(s)} \tag{41}$$

$$\frac{Y(s)}{N(s)} = -\frac{C(s) * G(s)}{1 + C(s) * G(s)} \tag{42}$$

Several conclusions can be drawn from the above transfer functions. First, the absolute transfer function of equations 39 and 42 are the same. As a result, all noise added by the AD converter will be seen as the physical force at the load cell. The frequency components might be less troublesome, but an offset in the load cell is not removed by the feedback model. It is therefore the task of the hitch connection group to carefully calibrate the load cell circuit. Secondly, the transfer of $\frac{E(s)}{R(s)}$ is the same as $\frac{Y(s)}{D_2(s)}$. Therefore, it is in the interest of both transfer functions to have a steady state value of zero.

The controller will be designed using the internal model based approach[13]. In the internal model base approach, there is one parameter, α, which determines the P and the I of the PI controller. The plant has 1 pole and no zeros. P and I are chosen in such a way, that the closed loop transfer is equation 43. The advantage is that the resulting closed loop system is only first order with properties that can easily be solved analytically instead of with the computer.

$$\frac{Y(s)}{R(s)} = \frac{\alpha}{s+\alpha} \tag{43}$$

The corresponding PI controller is:

$$\begin{aligned} C(s) &= K * (1 + \frac{1}{s * T_i}) \\ K &= \alpha/30 \\ T_i &= 1/30 \end{aligned} \tag{44}$$

The rise time is related to α in equation 45. A higher α is desired to increase the rise time. However, the slope is also increased, which can have negative effect on the comfort of the driving system.

$$t_r = \frac{2.3}{\alpha} \tag{45}$$

The sampling frequency is related to α in equation 46. A lower value of α results in a lower sampling frequency being possible. Reversely, the sample frequency limits the value of α.

$$\omega_s \geq 5 * \alpha \tag{46}$$

Alpha is chosen as 10. The resulting rise time is less than 0.6 seconds. In addition to that it is a factor three lower than the pole of the current control model. As a result, slight changes in the pole of the current control model have less effect. The sample frequency of 80 Hz is high enough for an alpha of 10.

3.2.3.5 Simulation Results

The hitch force controller is simulated with the minimum and maximum pole of the solenoid with the designed current control loop. The results are shown in table 5.

Table 5: current controller parameters

pole position	**rise time $\frac{Y(S)}{R(s)}$ [s]**	**phase margin [°]**	**gain margin**
pole at -250 (maximum)	0.2166	89.8	inf
pole at -875 (minimum)	0.2189	89.9	inf

Figure 10 shows the bode plots for the different poles of the solenoid. As can be seen from table 5 and the bode plots, the hitch control model almost responds identical to all poles. Both the phase margin and gain margin are high, because the phase of the plant can maximally be -90 °. The theoretical rise time is 2.3 seconds. The actual rise times are maximally 10 % from that value, which is acceptable.

3.2.3.6 Digital Implementation

The controller design in the previous section has been done in the s-domain. In order to implement the controller on a chip, the controller transfer function has to be converted to the digital domain. The bilinear transform is used to transfer equation 48 to equation 49.

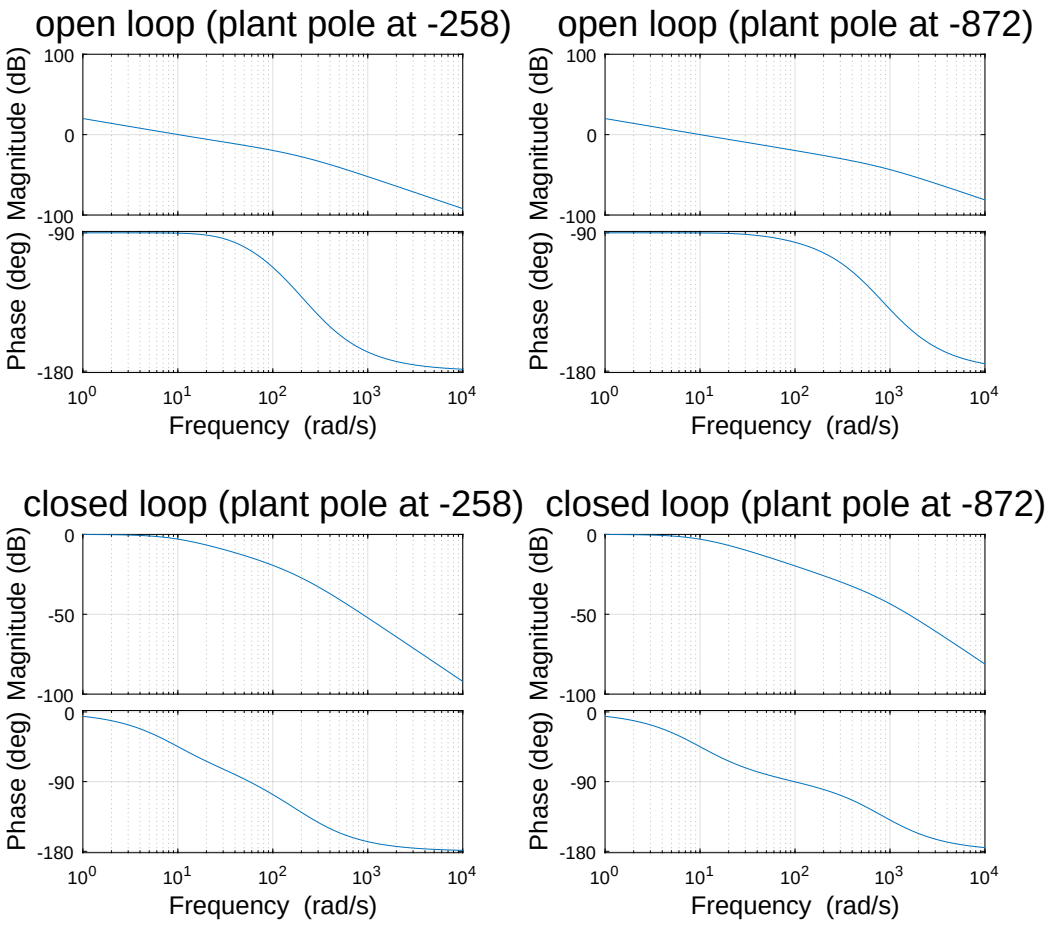

Figure 10: open loop and closed loop bode plots for the extreme poles of the solenoid for hitch force controller

$$s = \frac{2}{T} * \frac{1 - z^{-1}}{1 + z^{-1}} \ : \ bilinear\ transform \tag{47}$$

The following equation is the controller transfer function in the s-domain:

$$C(s) = \frac{\alpha}{I} + \frac{\alpha}{s} \tag{48}$$

The following equation is the controller transfer function in the z-domain:

$$C(z) = \frac{(\alpha * \frac{1}{I} * 2 + \alpha * T) + z^{-1} * (-\alpha * \frac{1}{I} * 2 + \alpha * T)}{2 * (1 - z^{-1})} \tag{49}$$

The pole of the transfer function is situated on the unit circle. That is expected, because an integrator is used. A saturation block is placed after the controller. Therefore a concept is introduced called anti-windup. Once the output of the controller crosses the maximum force, the output is set at the threshold value.

3.2.4 Microcontroller Implementation

The designed hitch force control model needs to be implemented in c and programmed on the E-connect. E-Trailer has designed a PCB with a microcontroller, an accelerometer and a gyroscope. The E-Connect, also called the main processing unit, is used for the digital implementation of the controller and to extract sensor data. The main processing unit communicates with the hitch control unit(HCU) and brake control unit(BCU). The HCU sends the load cell force and braking signal for the control algorithm. The main processing unit will transmit the calculated braking force to the BCU. The E-Connect is programmed in the C-language, since the code is implemented in the existing code of E-trailer, which is programmed in C.

The microprocessor of the E-connect is the Atmel SAM4E8E, a 32-bit microprocessor with most importantly 2 CAN-controllers, 2 UART connections and 3 three-channel timers. The 2 CAN-controllers are connected to CAN-transceivers to communicate with the other modules. The UART connections are used to debug and to log data. Furthermore the E-connect has three sensors, which will be explained in section 3.3.1. These will not be used for the hitch force control model, so the hardware provided is sufficient for this application.

In this section the overall structure of the implemented code is explained, starting with the communication, followed by an explanation of the structure of the code.

CAN-protocol

The CAN-protocol is a message-based communication protocol without a host, making it a more robust network. That is especially important in a safety-critical brake system. The CAN messages consist of 2 parts. The message property part is 44 bits and mainly consists of an ID, the length of the data and the type of message. The data part can vary in size from 0 to 64 bits. If the CAN-controller receives a CAN-message from the CAN-transceiver, then it compares the ID with pre-set masks from the receiving mailboxes embedded in the microcontroller. A mailbox is an asynchronous message queue. That means that the CAN-controller can store a message, so that the algorithm can process it a while later. The receiving mailboxes have a mask and ID. If equation 50 is true, then the message is placed in that specific mailbox. Two things can happen. The algorithm can poll the data or an interrupts is generated so the algorithm can process the data. In figure 11 the distribution of the mailboxes is shown.

$$ID_{mailbox} \,\&\, mask_{mailbox} == ID_{message} \,\&\, mask_{mailbox} \tag{50}$$

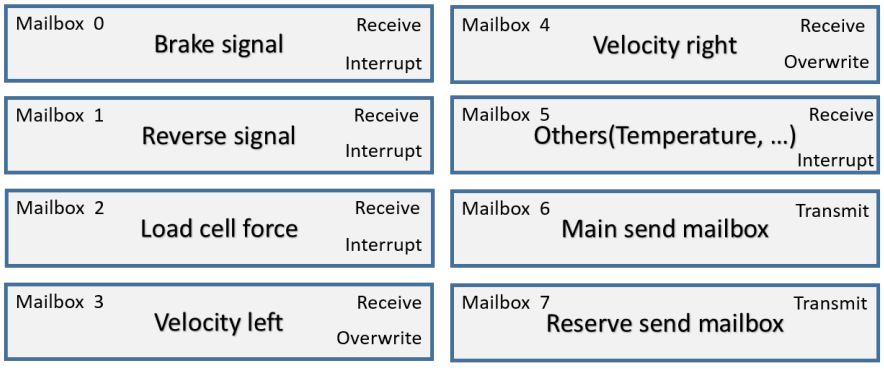

Figure 11: The distribution of the mailboxes with the type included

As can be seen at mailbox 3 and 4, these mailboxes will not generate an interrupt. This is done so the algorithm can decide when to read the speeds. The speed is not needed every time it is send to the microcontroller, so only the most recent value is used. The other receiving mailboxes do generate an interrupt. In order to send data, the ID, data length and data has to be given to

the transmitting mailboxes. After that, the mailbox can send the data based on priorities via the CAN-transceiver.

Structure Code

Requirement 4.1.1 of the RDW, explained in chapter 2.3, states that the system should respond in 0.6 seconds. The goal of the microcontroller is to take the least time possible, so the control algorithm can fully control the speed of the response. To achieve this the microcontroller functions mostly on interrupts. As can be seen in figure 12, on start-up the microcontroller starts with initialising all sensors and the communication: CAN, I^2C and UART. After that the microcontroller pauses for 1 second. In the mean time, the hitch connection module is done initialising and broadcasts the hitch force. With this method, the microcontroller will not time out, because it does not receive a load cell value, something which will be explained later.

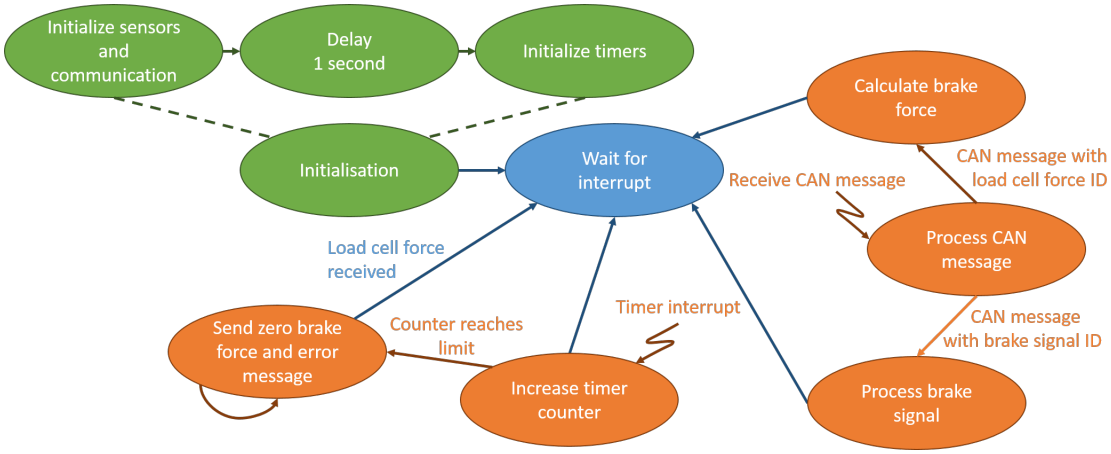

Figure 12: The structure of the implementation of the controller and processing of the in and outputs. Blue means functions in the main function, orange are interrupts and green is initialising

After 1 second delay, the interrupts for the CAN communication timer used for interrupt time outs is initialised and started. When the initialisation is finished, the microcontroller keeps waiting for an interrupt, either from a received CAN message or a timer interrupt.

First the timer interrupt is explained. This interrupt is generated each time the timer reaches its limit, which happens at the same frequency as receiving a new load cell value. The interrupt causes a counter to increase by one. When the value of the timer exceeds a limit of 10, it means that the microprocessor expected 10 load cell values, but did not receive any. In that case the microprocessor will send a brake force of zero, so the driver can safely pull over his vehicle to the side of the road. An error message is send via the CAN-bus. If a new load cell force is received, then the microcontroller returns to its original state.

Receiving a CAN-message also generates an interrupt. All interrupts of a CAN-controller are handled by the same interrupt handler, the workflow of this handler is shown in figure 13. It starts by checking what kind of interrupt is generated. If it is an mailbox interrupt, then each mailbox is checked for an interrupt flag. If the flag is high and the mailbox is an receiving mailbox, then the mailbox is checked if it is ready to receive a CAN message. If all restrictions are met, then the corresponding function from a function pointer array is executed. A function pointer array is chosen for easier future use for the company, since it keeps the code easy to read and it makes it easier to change or extend the amount of functions an mailbox can call.

The function that is called when receiving a CAN-message with the ID of the brake signal, changes a global variable into the value of the message. In that way the microcontroller knows

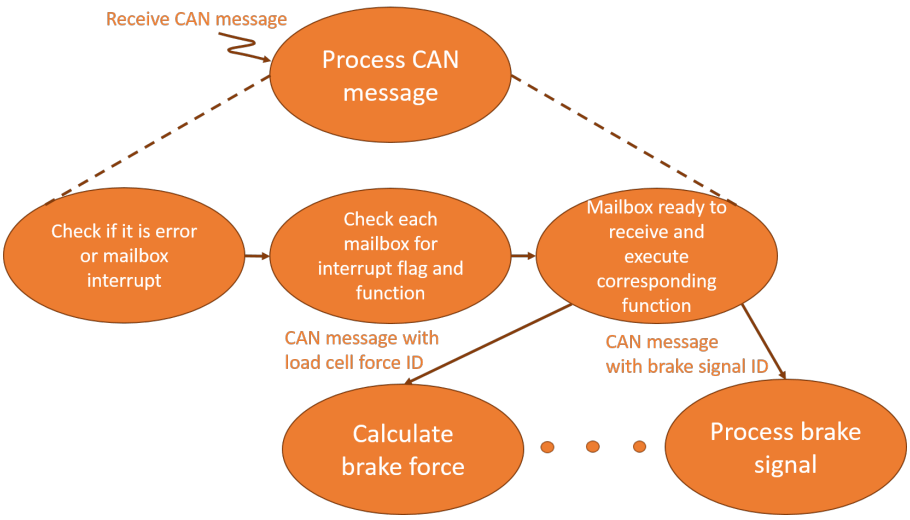

Figure 13: An overview of the function that handles the can interrupts

at all times what the value of the brake signal is. The processing of a CAN-message with the ID of the load cell force is illustrated in figure 14.

First, the data needs to be converted from an integer representation to a decimal/float representation. After that, the transfer function of the controller is applied, which leads to a temporary brake force. This force must be bounded by the saturation limits, because the brakes can not handle more force. Then there is checked if the brakes of the car are applied. If that is the case, then the temporary brake force becomes the real brake force, otherwise the brake force will become zero. The final steps are to store the current brake force as previous brake force and send the force via CAN to the brake control units.

3.3 Problem Statement 2: "Identify the sensors and methods needed for sway detection"

The second goal of the thesis is problem statement 2: Identify the sensors and algorithms needed for sway detection. Firstly, an overview is given of the range of sensors that can be applied for sway detection. Secondly, several top level algorithms are described that can be used for sway detection. Two of the useful sensors are the accelerometer and the gyroscope. The E-Connect, a device produced by E-Trailer is equipped with an accelerometer and gyroscope. The accelerometer and gyroscope of the E-Connect are compared with other sensors on the market. After that, an calibration algorithm is explained that transforms the sensor data to the earth's and trailer's reference frame. Next, the orientation model is discussed that uses filtering to predict the orientation of the trailer. Due to the limited time and the dangerous nature of swaying, no tests were carried out to collect sensor data during swaying. Therefore the aim of problem statement 2 is not to provide a solution. A start is made with processing key sensor data, which future groups can use to design the actual algorithm.

3.3.1 Sensor Overview and Top Level Algorithms

Before designing an algorithm, first an overview must be given of the available sensors to detect swaying. Swaying is a oscillatory movement of the trailer behind a vehicle. In order to detect oscillations, either the angle or the angular velocity needs to be known. There are no sensors available that directly measure the angle with respect to the car. However, there are gyroscopes on the market that measure the angular velocity in three dimensions. Another way of detecting

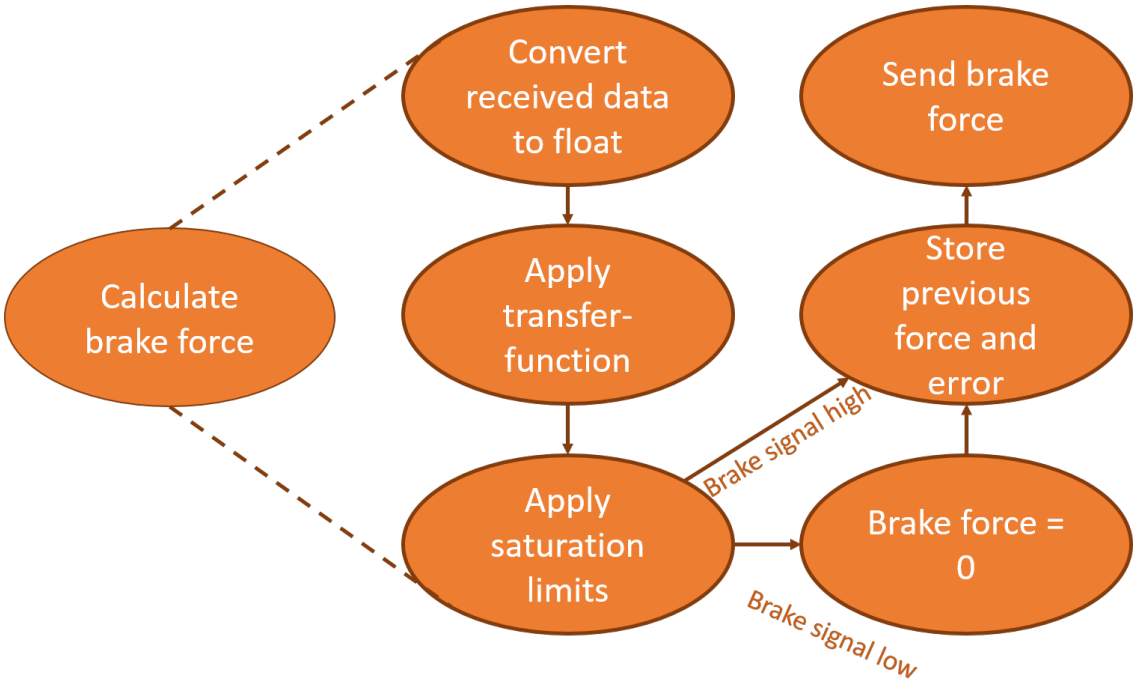

Figure 14: A structural overview of the function that implements the controller

movement with respect to the car is to use a camera on the trailer that points to the car. The disadvantage of a camera is that they are expensive and that they get dirty, since all dirt is collected at the front of the trailer. As a result, the implementation with the gyroscope is preferred. The allowed swaying is also dependent on velocity. At high speeds, the trailer should not turn quickly, whereas at high speeds, it may.

There are two models that can be implemented with the gyroscope and the accelerometer. The first model uses a threshold for the angular velocity based on the velocity at which the trailer moves. If the threshold is passed, then swaying is detected. The advantage of the model is that it is simple. The disadvantage is that noise might result in spikes that pass the threshold when there is no actual swaying. A low-pass filter could be a solution to that problem. The second model uses the accelerometer and gyroscope to estimate the orientation of the trailer. Oscillations of the trailer car combination might occur at specific frequencies. Filters can be used to identify the "signal power" of a certain frequency band and if a certain threshold is reached, then there is swaying. The signal processing can either be done on the angle or the angular velocity. Figure 2 in the literature study shows the dependence of yaw rate versus the velocity. Points above the curve are regarded as swaying and points underneath the curve are regarded as safe and normal driving. The curve can be constructed by carrying out swaying tests with different masses. It is expected that the natural swaying frequency of the car trailer will be mass dependent. Therefore, tests must be carried out with different masses.

Another approach is to use the centripetal force of the trailer to indicate whether there are oscillations or not. The same methods can be applied as the previous paragraph. A velocity-centripetal force graph will be created that denotes a safe zone and dangerous zone. The advantage is that only two sensors are needed instead of three. The gyroscope sensor also needs the accelerometer for calibration.

The problem with the E-Connect is that the module can be mounted in any direction. Therefore a calibration algorithm has to be constructed that transforms the sensor data to the correct reference frame.

The velocity can be measured with different sensors. A tachometer is used to count the number of rotations of a wheel. The velocity is calculated by dividing the circumference of the wheel by the time period of the rotation. The advantage is that both the circumference and the time period can be estimated rather accurately. The disadvantage is that at low speeds, the sample frequency is low and less precise. Another way of measuring the velocity is the GPS. The GPS is known for position measurement, but the velocity can also be directly extracted from the sensor. The accelerometer can be used to estimate velocity differences between sample points. However, it can only be used combined with a velocity sensor. The algorithms discussed in the section of problem statement 2 are the calibration model and the orientation model.

3.3.1.1 Accelerometer

The acceleration sensor on the E-connect is the ST microelectronics lsm303d[15]. This sensor is compared with the ST microelectronics LSM330DLC[16] and the sparkfun MPU-6050[17].

Table 6: Analysis acceleration sensor

	LSM303D	**LSM330DLC**	**MPU-6050**
Range [g]	$\pm 2, \pm 4, \pm 6, \pm 8, \pm 16$	$\pm 2, \pm 4, \pm 8, \pm 16$	$\pm 2, \pm 4, \pm 8, \pm 16$
Offset [mg]	± 60	± 60	± 50 (x and y axis) ± 80 (z azis)
Noise density [$\mu g/\sqrt{Hz}$]	150	220	400
Price[€]	1.31	4.21	11.86

The MPU-6050 is significantly more expensive, because the chip includes a digital motion detection unit, which can recognise programmable 3D-motions and gestures. That feature is not necessary for the system. The ST microelectronics LSM303D is the best choice as accelerometer, because the user can choose from more ranges with less noise and a lower price.

3.3.1.2 Gyroscope

The used gyroscope is the ST microelectronics L3GD20[18]. It is compared with the ST microelectronics LSM330DLC[16] and the sparkfun MPU-6050[17].

Table 7: Analysis gyroscope sensor

	L3GD20	**LSM330DLC**	**MPU-6050**
Range [°/s]	$\pm 250, \pm 500, \pm 2000$	$\pm 250, \pm 500, \pm 2000$	$\pm 250, \pm 500, \pm 1000, \pm 2000$
Offset[°/s]	$\pm 10, \pm 15, \pm 75$	$\pm 10, \pm 15, \pm 25$	± 20
Noise density [$^\circ/s/\sqrt{Hz}$]	0.03	0.03	0.005
Price[€]	1.91	4.21	11.86

The maximum angular velocity of the gyroscope is $\pm 90^\circ/s$. In that case, the trailer maximally rotates ones per four seconds. A car is not able to make such movements. A range of $\pm 250^\circ/s$ is chosen, in that case the MPU-6050 has more offset, but a lower noise density than the L3GD20 and he LSM330DLC. The difference in noise does not compensate for the larger price, so the company chose the right sensor.

3.3.1.3 Magnetometer

The used sensor, the ST microelectronics LSM303D[15], is compared to the NXP MAG3110[19] and the NXP FXOS8700CQ[20].

Table 8: Analysis magnetometer

	LSM303D	**MAG3110**	**FXOS8700CQ**
Range [μT]	$\pm 200, \pm 400, \pm 800, \pm 1200$	± 1000	± 1200
Offset [μT]	-	± 100	± 10
Noise density [μT/RMS]	0.5	0.4	0.3 - 1.5*
Price[€]	1.31	1.11	2.00

* (depending on operation mode)

The ST microelectronics LSM303D is appropriate when a higher sensitivity is needed(for a range of $\pm 200 \mu T$). Otherwise the NXP MAG3110 is a better choice, due to the better noise performance and price. Since the function of the sensor is not yet determined the correct sensor can not yet be chosen.

3.3.1.4 GPS

The GPS unit GP-20U7[21] is implemented by E-Trailer on the development board. The performance parameters are shown in table 9. The circular error probable(CEP) is a stochastic performance indicator of GPS sensors. It is the radius of a circle around the true position where 50 % of the measurements are located. The time to first fix (TTFF) is the time required for the GPS unit to determine the position, time and velocity. The GPS sensor cannot be used for precise positioning within a meter. The measured velocity of the GPS is rather precise. It has an accuracy of 0.1 m/s or 0.36 km/h. That is precise enough for the anti-sway detection.

Table 9: GPS accuracy

parameter		**unit**
CEP	2.5	[m]
velocity	0.1	[m/s]
TTFF		
- hot start	1	[sec]
- warm start	28	[sec]
- cold start	29	[sec]

3.3.2 Orientation Model

The orientation model takes the acceleration and gyroscope data to predict the current orientation of the trailer with respect to the Earth. In addition to that, the dynamic acceleration can be estimated, which can be used for the sensor fusion model. The sensor might be mounted in any direction. Therefore a calibration model is explained first that transforms the data from the sensor's reference frame to the trailer's reference frame. Due to the calibration model, the gyroscope can be used for the anti sway algorithm. After that, the orientation model itself is explained and verified with test results.

3.3.2.1 Reference Frames

Before explaining the orientation model, it is important to identify the different reference frames. There are three reference frames: the earth's reference frame, the trailer's reference frame and the sensor's reference frame. The measurements of the sensor are in the sensor's reference frame. The sensor's reference frame is that of the E-Connect, which is shown in figure 15. The trailer's reference frame takes as X-direction the direction of the car, see figure 16.

3.3.2.2 Euler Angles

The earth's reference frame is identified in terms of Euler angles. The concept of Euler angles has its roots in aerospace engineering. The angles indicate the relative orientation of the aeroplane

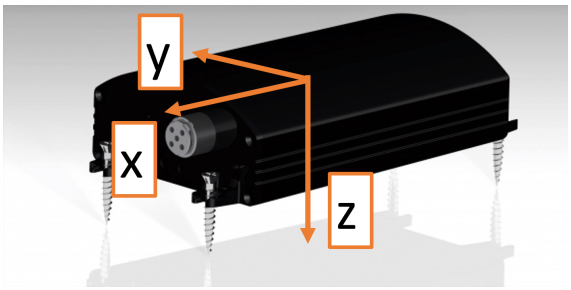

Figure 15: convention of axis of the sensor reference frame

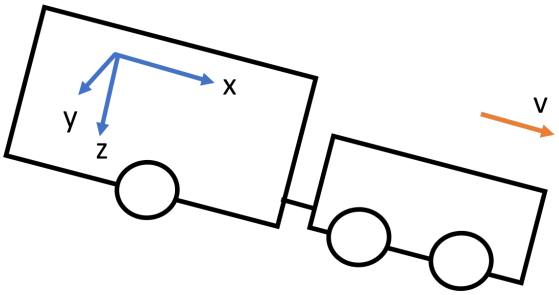

Figure 16: convention of axis of the trailer's reference frame

with respect to the earth. There are three angles: the pitch, the roll and the yaw. The directions of these angles are shown in figure 17 [22]. The pitch angle is interesting in the mountains, since it indicates the slope angle. The yaw angle can be used for the sway detection algorithm.

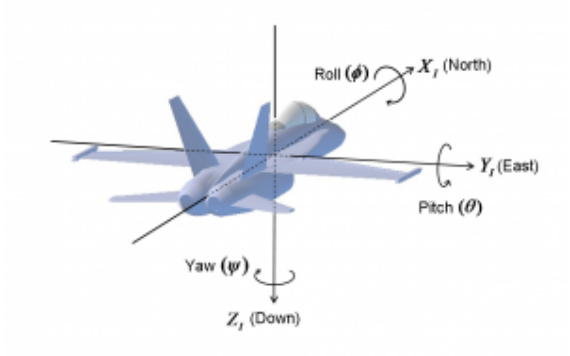

Figure 17: Euler angles

3.3.2.3 System Decomposition

The orientation model uses the accelerometer and gyroscope to obtain the relative orientation to earth using Euler angles(see paragraph 3.3.2.2). Figure 18 shows the block diagram of the orientation model. The gyroscope measures angular velocity, which needs to be integrated to obtain the Euler angles. In the digital domain, that corresponds to a multiplication with Δt. An algorithm has to be designed to convert the acceleration vector to Euler Angles. As the sensor can be mounted in any way in the caravan, a calibrating algorithm has to be designed to be able to convert the acceleration vector to Euler angles. The calibration algorithm is discussed in paragraph 3.3.2.4. The accelerometer measures the sum of the gravity vector and the dynamic acceleration vector. In order to determine the Euler angles, ideally one only wants the gravity vector. However, the dynamic acceleration is a noise source in the short term. By using a low-

pass filter, the dynamic acceleration is filtered and the gravity vector remains. The gyroscope has a certain offset and possibly a scale factor error in the measurement. Therefore, it is accurate in the short term, but inaccurate in the long term. A high-pass filter is used to remove the offset of the gyroscope. The result is a complementary filter, where the acceleration sensor is the long term predictor of the gravity vector and the gyroscope measures the relative angle difference from the gravity vector. The summation of both provides an estimation of the Euler angles. In order to obtain the dynamic acceleration vector, the gravity vector has to be subtracted. The previously calculated Euler angles can be converted to the gravity vector. The magnitude is 9.81 m/s^2. To calculate the dynamic acceleration, first a low-pass filter has to be designed to remove the high frequency noise. Secondly, the gravitation vector has to be subtracted and the acceleration vector remains.

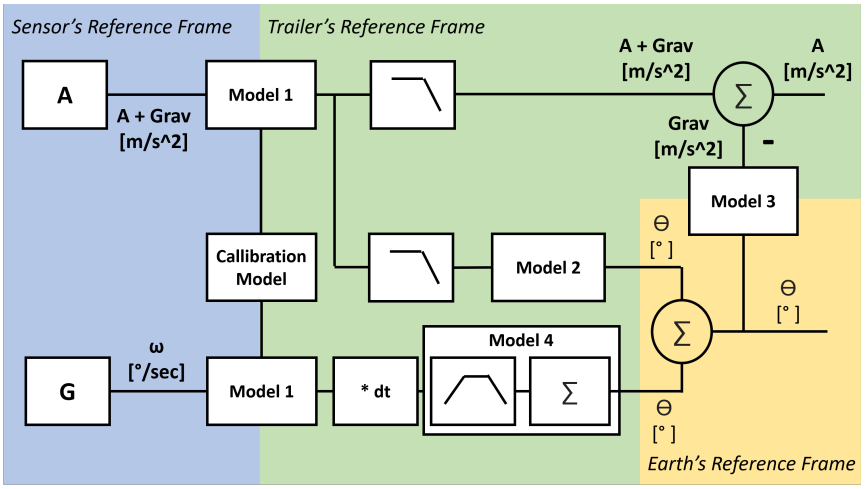

Figure 18: orientation model

3.3.2.4 Calibration Model

The main processing unit of the E-Brake can be mounted in any position in the trailer at any angle. As a result, the sensor axis are not aligned with the orientation of the trailer. Therefore, an orientation algorithm has to be applied to rotate the incoming vectors. Two steps have to be taken to determine the angle of the trailer.

Step 1:

- Level the trailer such that the pitch and roll are zero degrees and the trailer does not move.

Step 2:

- Move the hitch connection upwards to indicate the front of the trailer

$$\begin{aligned} F_1 &: levelled\ accelerometer\ measurement \\ F_2 &: accelerometer\ measurement\ movedupwards \\ F_3 &: orthogonal\ vector\ to\ F_1\ and\ F_2 \\ F_4 &: orthogonal\ vector\ to\ F_1\ and\ F_3 \\ u_x, u_y, u_z &: unit\ vectors\ of\ new\ coordinate\ system \end{aligned} \tag{51}$$

Figure 19 shows multiple vectors that are important for the calibration algorithm. The goal is to find the unit vectors of the trailer's reference frame. Force F_1 is the levelled acceleration measurement. Therefore, it is also the z-direction of the trailer's reference frame(see equation 52). The

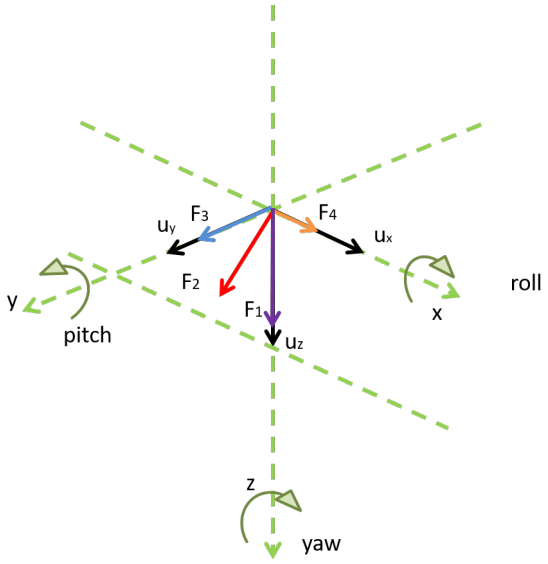

Figure 19: calibration upward orientation

second measurement, with the trailer at an angle, results in vector F_2. The only plane in which vector F_2 can be present, is the xz-plane. The unit vector y of the trailer's reference frame can be calculated by calculating the outer product of F_1 and F_2(see equation 53). From the two unit vectors u_z and u_y, the third unit vector u_x can be calculated(see equation 54).

$$u_z = \frac{F_1}{||F_1||} \tag{52}$$

$$u_y = \frac{F_2}{||F_2||} \times u_z \tag{53}$$

$$u_x = u_y \times u_x \tag{54}$$

3.3.2.5 Model 1

The calibration algorithm designs the axis of the trailers reference frame relative to the sensor's reference frame. Equation 55 shows the projection of the sensor's vector to the trailer's reference frame. The vector v_{in} denotes the input sensor data vector and the vector v_{out} is the rotated sensor data vector.

$$v_{out} = [v_{in} * u_x, v_{in} * u_y, v_{in} * u_z] \tag{55}$$

3.3.2.6 Model 2

The following two vectors are the projections of on the xz-plane and the yz-plane.

$$\begin{aligned} F_{2,projonxz-plane} &= F_2 - \frac{F_2 * u_y}{||u_y||^2} u_y \\ &= F_2 - (F_2 * u_y) u_y \end{aligned} \tag{56}$$

$$F_{2,projonyz-plane} = F_2 - \frac{F_2 * u_x}{||u_x||^2} u_x = F_2 - (F_2 * u_x) u_x \tag{57}$$

The following equations are used to calculate the pitch and roll angles at a given angle force F_2.

$$\theta_{pitch} = cosd^{-1}\Big(\frac{F_{2,proj\ on\ xz-plane} * u_z}{||F_{2,proj\ on\ xz-plane}|| * ||u_z||}\Big) = cosd^{-1}\Big(\frac{F_{2,proj\ on\ xz-plane} * u_z}{||F_{2,proj\ on\ xz-plane}||}\Big)\Big) \tag{58}$$

$$\theta_{roll} = cosd^{-1}\Big(\frac{F_{2,proj\ on\ yz-plane} * u_z}{||F_{2,proj\ on\ yz-plane}|| * ||u_z||}\Big) = cosd^{-1}\Big(\frac{F_{2,proj\ on\ yz-plane} * u_z}{||F_{2,proj\ on\ yz-plane}||}\Big)\Big) \tag{59}$$

Equations 58 and 59 only calculate the absolute value of the pitch and roll angle. The sign has to be added according to the following rules:

$$\begin{aligned} &If\ F_{measured} * u_x > 0 \rightarrow pitch\ is\ negative \\ &If\ F_{measured} * u_x < 0 \rightarrow pitch\ is\ positive \\ &If\ F_{measured} * u_y < 0 \rightarrow roll\ is\ negative \\ &If\ F_{measured} * u_y > 0 \rightarrow roll\ is\ positive \end{aligned} \tag{60}$$

3.3.2.7 Model 3

The final step is to convert the Euler angles to a gravity vector in the trailer reference frame. Therefore, the tangential component in the x direction has to be calculated. The first step is to write the relationships between the pitch, roll and the magnitude of the gravity vector.

$$tan(\theta_{pitch}) = \frac{-g_x}{g_z} \tag{61}$$

$$tan(\theta_{roll}) = \frac{g_y}{g_z} \tag{62}$$

$$|g| = \sqrt{g_z^2 * tan^2(\theta_{pitch}) + g_z^2 * tan^2(\theta_{roll}) + g_z^2} \tag{63}$$

$$|g_z| = \frac{1}{\sqrt{tan^2(\theta_{pitch}) + tan^2(\theta_{roll}) + 1}} \tag{64}$$

Under the assumption that the roll and pitch are less than 90 degrees, the following equations hold:

$$\begin{aligned} g_z &= |g_z| \\ g_y &= |g_z| * tan(\theta_{roll}) \\ g_x &= -|g_z| * tan(\theta_{pitch}) \end{aligned} \tag{65}$$

3.3.2.8 Model 4

The gyroscope measures the angular velocity. That is integrated to obtain the angle difference relative to the first measurement. The measured angular velocity $\hat{\omega}_n$, contains an offset α and a noise vector N due to quantisation errors and distortion. For now, it is assumed to have zero mean and a volatility σ.

$$\hat{\omega}_n = \omega_n + \alpha + N\ ,\ \alpha\ : angular\ offset,\ N(0, \sigma^2)\ :\ Noise \tag{66}$$

The angle θ used in context with the gyroscope, will be the estimator of the angle difference relative to the gravity vector.

$$\theta_{n+1} = \theta_n + \omega_n * \Delta t \tag{67}$$

As it is an estimator, it can be rewritten as:

$$\theta(z) = H_1(z) * (\omega * \Delta t)(z) \tag{68}$$

$$H_1(z) = \frac{1}{1 - z^{-1}} \tag{69}$$

The following equation shows the effect of the high-pass filter $H_2(z)$. $\theta(z)$ is the input and $\hat{\theta}(z)$ is the output.

$$\hat{\theta}(z) = H_2(z) * \theta(z) \tag{70}$$

The two filters $H_2(z)$ and $H_1(z)$ can be combined to avoid storage of the intermediate value $\theta(z)$. The major advantage is that the intermediate variable can go to infinity due to the offset of the angular velocity. The high-pass filter can compensate that theoretically, but practically, going to infinity is not an option.

$$H_{tot}(z) = H_2(z) * H_1(z) = H_2(z) * \frac{1}{1 - z^{-1}} \tag{71}$$

$$H_2(z) = \frac{b_2(z)}{a_2(z)} = \frac{b_2(1) + b_2(2) * z^{-}1 + ... + b_2(n_b + 1) * z^{-n_b}}{1 + a_2(2) * z^{-1} + ... + a_2(n_a + 1) * z^{-n_a}} \tag{72}$$

$$H_{tot}(z) = \frac{b_2(z)}{a_2(z) * (1 - z^{-1})} = \frac{b_2(z)}{a_2(z) - z^{-1} * a_2(z)} \tag{73}$$

$$b_{tot} = [b_2, 0], \;\; a_{tot} = [a_2, 0] - [0, a_2] \tag{74}$$

3.3.2.9 Anti-Aliasing Filter Parameters

The acceleration sensor and the gyroscope need to be configured before using them. The available configurations are shown in table 10 and 11. For the acceleration sensor, the sample rate and anti-aliasing low-pass filter need to be configured. For the gyroscope, the sample rate, anti-aliasing low-pass filter and a high pass filter need to be selected. The sample rate will be designed within the range of 20 to 100 Hz. The maximum frequency component will be 2 Hz. Still a multiple of that needs to be the sample rate to respond on time. The lowest anti aliasing low-pass frequency of the accelerometer needs to be selected, which is 50 Hz. As a result, the data rate can be configured as 100 Hz and the frequency at which the sensor is read can be determined later. For the gyroscope, the anti aliasing low-pass filter is set at 12.5 Hz, the lowest frequency configurable. The analog high-pass filter can be bypassed. The decision is made to digitally implement the high-pass filter. The data rate of the gyroscope will be the lowest available, which is 95 Hz.

Table 10: acceleration configurable parameters

Data Rate [Hz]
100
50
25
12.5
Anti Aliasing Filter [Hz]
50
194

Table 11: gyroscope configurable parameters

Data Rate [Hz]
95
190
380
760
Anti Aliasing Low-pass Filter [Hz]
12.5
25
50
70
100

3.3.2.10 Simulation Results

Multiple tests have been done to verify the model. Sensor data was collected by driving a car with a trailer behind. In this section, the different sub-parts of the orientation model will be discussed first. Secondly, the gyroscope sensor behaviour will be analysed by providing graphs of the sensor data after and before filtering. After that, the data processing of the accelerometer both for the dynamic acceleration and the estimation of the Euler angles are explained. The final conclusion will give recommendations about improvements that can be made.

Several tests are carried out to identify how the sensors and the model relate to each other. One test will be used to evaluate all parts of the orientation model. First, the E-Connect with the accelerometer and gyroscope was mounted in the trailer in an arbitrary direction. After that, the trailer was calibrated by following the procedure of section 3.3.2.4. A car was used to tow the trailer for approximately 20 minutes. First, the trailer turned 11 times to the right and after that 7 times to the left. Directly after the first, third, fifth and seventh turn, the car went upwards with approximately 5 degrees and downwards with approximately 5 degrees at a hill. The final turns were done on a horizontal road.

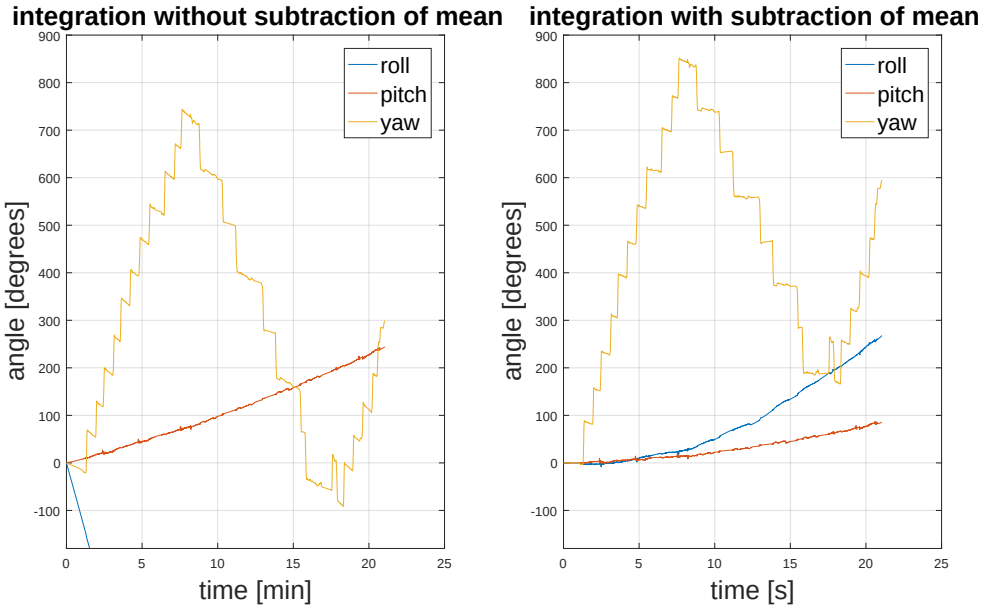

Figure 20: angular velocity integrated

Figure 20 shows the integrated angular velocity without filtering. The result is an angle relative

to the start position of the trailer. As can be seen in both pictures, there is a drift of the sensors due to an offset of the angular velocity, which can vary in time. The left picture is the integration of the actual raw data. The drift term can be estimated by taking the average of the gyroscope value of the first 2 seconds, when the car does not move. That drift term can be subtracted from the incoming gyroscope data. The right graph shows the integrated angle with drift compensation. The following conclusions can be drawn from both graphs:

1. The drift term is time dependent and can not be determined by a single measurement;
2. The yaw angle changes are clearly visible at turns;
3. The pitch and roll changes are not clearly visible at a hill;
4. The drift does not rise from integrating noise, but from the offset of the angular velocity;
5. The cutoff frequency of the high-pass filter should be maximally 0.025 Hz;
6. The calibration algorithm works correctly;

Conclusion 4 requires more explanation. Integrating noise results in an angle which goes up and down. However, the integrated pitch angle continuously goes up and the integrated yaw and roll almost always goes down, except during turns of the trailer. Therefore, there is no clear integration of noise. The calibration model works correctly. If the calibration model does not work correctly, then a part of the yaw angle would appear in the roll or pitch. That is not visible in the graph at turns. Therefore, the calibration model works correctly.

The challenge is to chose a cutoff frequency for the complementary filter. A turn typically takes between 5 and 10 seconds. In order for the high pass filter of the gyroscope to predict the entire turn in Euler angles, the cutoff frequency has to be $1/4$ of the time that a turn takes. That equals a cutoff frequency of 0.025 Hz. There is also a minimum cutoff frequency determined by the time dependency of the drift. The Fast Fourier Transform has been performed on the integrated roll angle. The result is shown in figure 21. All windows give similar results, but the rectangular window is used, because it has the smallest main lobe width. After 0.5 Hz, the single-sided amplitude spectrum stays low. Based on figure 21 the minimum cutoff frequency should be 0.05 Hz. That creates a conflict with the minimum cutoff frequency of the high-pass filter based on the time a turn takes.

The raw sensor data from the accelerometer is not easy to analyse or process due to the large amount of noise added to the signal. The noise partially comes from the sensor and partially from the trailer moving up and down due to irregularities of the road. Therefore, a filter has to be designed that removes the high frequency components that are not part of the "system" to be analysed. A 2^{nd} order low-pass filter is used with a cutoff frequency of 0.7 Hz. The raw data is shown in the left graph of figure 22. The filtered acceleration data is shown in the right graph of figure 22. The following conclusions can be drawn from both graphs:

1. The up and down movement of the trailer due to irregularities of the road average to zero;
2. The centripetal force in the y direction is visible in both plots;
3. The average value of the acceleration in the x-direction can be assumed to be zero due to the acceleration and deceleration;
4. In order to remove more noise in the z-direction, the cutoff frequency should be decreased;
5. It cannot be stated that the acceleration is higher or lower than the deceleration in general;

The question is whether the acceleration itself can be used to estimate the Euler angles. An incorrect estimation of the Euler angles result in the gravity vector being projected in the x- and y-direction acceleration vectors. If that happens, the dynamic acceleration output of the orientation model will be incorrect. Small changes in the Euler angles will not result in a lot of disturbance. An error of 4 $^\circ$ introduces an acceleration disturbance of approximately 0.6 m/s^2. That is

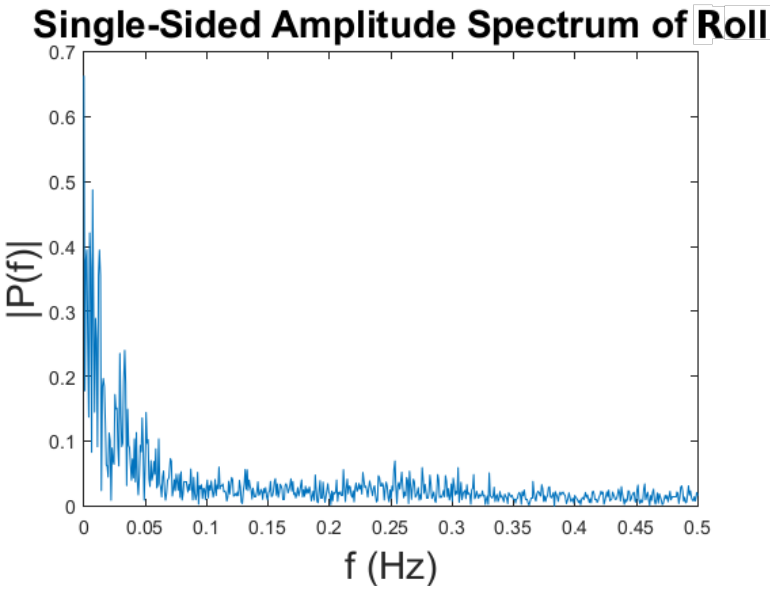

Figure 21: Fast Fourier Transform of the integrated roll angle

acceptable. Figure 23 shows the Euler angles calculated from the accelerometer with a low pass filter with different frequencies. Between t = 10 min and t = 20 min, there are 4 tops and valleys visible. These correspond to driving up and downhill of a hill with a slope of approximately 3 to 7 degrees. The other tops and valleys correspond to the effect of the car-trailer combination accelerating and decelerating. The best results are obtained if the cutoff frequency is equal to 0.01. Higher cutoff frequencies result in the acceleration and deceleration being visible in the Euler angles, whereas lower frequencies do not detect the inclinations. The following conclusions can be drawn from all graphs:

1. Limited acceleration filtering can result in wrong Euler angle prediction of maximally 5 to 10 degrees;
2. If only an accelerometer is used to estimate the Euler angles, then an error is introduced of maximally 2 to 3 degrees with fc = 0.01;
3. The quality of detecting a slope depends on the ratio between the time driving at a slope and the cutoff frequency of the filter;

3.3.2.11 Conclusion

The question is how to implement sway detection and provide the sensor fusion algorithm with the acceleration in the x-direction of the trailer. The calibration part of the orientation model works. The sensor data from the gyroscope and accelerometer can be transformed to the different reference frames. The next step is to identify the best sway detection algorithms. Both the yaw rate and the centripetal force can be used to determine whether the trailer sways or not. Future testing should identify which data is more robust. A velocity sensor has to be implemented, because the allowed turning and swaying depends on the velocity that the trailer has. The simulation results of the yaw rate are promising and for a threshold algorithm, the drift should not impose much problems. A high pass filter with a very low cutoff frequency can be implemented that removes the drift. The implementation of the orientation model is more difficult. The pitch changes in the gyroscope are not visible at a hill. The orientation model is designed on the edge of the precision of the sensors. There should be looked into why the pitch changes are not visible

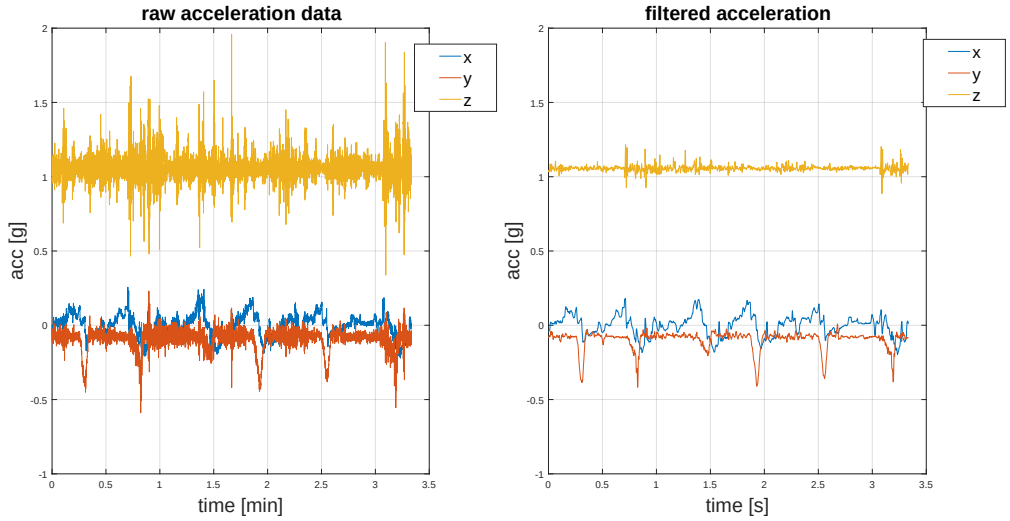

Figure 22: raw rotated acceleration data(left), filtered rotated acceleration data(right)

in the gyroscope data. The sample rate of the sensors have been limited to 100-200 Hz, because the microcontroller could not process the data without a large revision of the code. The anti-aliasing filter of the accelerometer is 50 Hz. At this point, it is sampled with 100 Hz. Increasing the sample rate increases the precision of the measurement. The same holds for the gyroscope. The sample rate can be increased to 380 Hz. The question is whether a higher sample rate makes the integrated angular velocity better.

3.4 Problem Statement 3: "Designing a Sensor Fusion Algorithm"

The third goal of the thesis is problem statement 3: Identify the qualities of the sensors to design a sensor fusion algorithm. There are multiple sensors that can be used to estimate the velocity of the trailer: the tachometer, the GPS sensor and the accelerometer. The GPS sensor is known for the position measurement. However, it is often forgotten that the velocity can be measured directly as well. First, the pros and cons of all sensors will be pointed out. After that, the fusion algorithm will be explained at a high level. The focus of the project was not to design a GPS unit. E-Trailer worked on a GPS unit that could be connected to our E-Connect and tachometer. However, they were unable to finish it on time. Therefore the design will only be described at a high level without empirical data.

3.4.1 Sensor Analysis

Before designing a fusion algorithm, the qualities of the different sensor sets need to be identified. The tachometer is not calibrated well. That means that the scaling factor of the velocity is not equal to one. In addition to that, at lower speeds, the velocity is less often updated than at higher speeds. The advantage is that the sensor will always give an output signal. The GPS sensor measures the velocity directly. The advantage is that it is precise with about 0.1 m/s. The disadvantage is that the sensor does not function correctly in tunnels or close to other objects that cause distortion. The question is also whether the resolution of 0.1 m/s is reached at low speeds. That has to be verified during testing. The third sensor is the accelerometer. The acceleration can be integrated to get an estimation of the velocity. Unfortunately, noise is also integrated. That means that in the short term, the accelerometer can accurately predict velocity differences, but in the long term not.

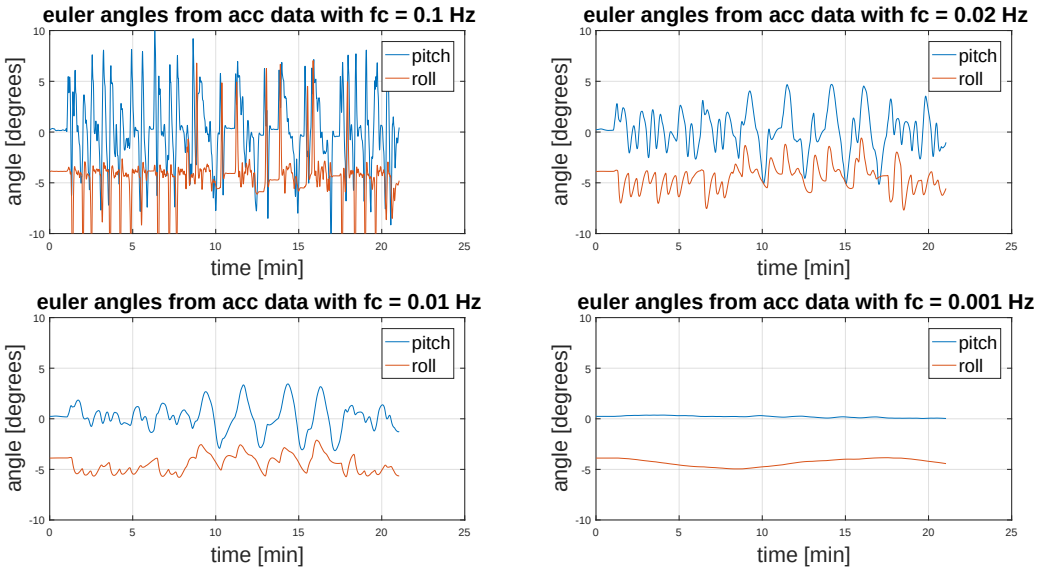

Figure 23: Euler angles from acceleration data with different LPF cutoff frequencies

3.4.2 Fusion Algorithm

A fusion algorithm will be designed that takes into consideration the strengths and weaknesses of all sensors. The bottleneck is that the GPS sensor is more precise, but not reliable and that the tachometer is less precise, but reliable. In addition to that, the accelerometer can be used to give a short term approximation of the velocity.

3.4.2.1 Decentralised Kalman Fusion Algorithm

The decentralised Kalman filter fusion algorithm designed by Shu-Li Sun and Zi-Li Deng[23] will be used. The difference between the centralised and decentralised Kalman filter is that the decentralised version supports multiple sensors that estimate the same parameter and the centralised does not. If the sensors are ideal, then the centralised version behaves better, but if one sensor fails, then the decentralised version behaves better. It is expected that the GPS sensor can behave unexpectedly and therefore the decentralised version is more suitable.

Figure 24 shows the layout of the decentralised Kalman filter. Every sensor has it's own Kalman filter with fault detection to determine whether a sensor functions or not. The estimated variance can be used to determine whether the sensor works accurately. The first layer calculates the cross covariance between the different sensor data. The second layer uses the cross covariance and the estimations to make a prediction of the states and the output covariance matrix. The weighted average formula is equation 75. The weights A_i depend on the cross covariance matrix.

$$\hat{x}_o = A_1 * \hat{x}_1 + A_2 * \hat{x}_2 + ... + A_l * \hat{x}_l \tag{75}$$

There are two ways of modeling the system that have their advantages and disadvantages. The first model defines the accelerometer as an input of the system. There is only one state, the velocity. The process noise is related to the inaccuracy of the orientation model. The second model defines two states: the acceleration and the velocity. The acceleration is assumed to vary in a Gaussian manner.

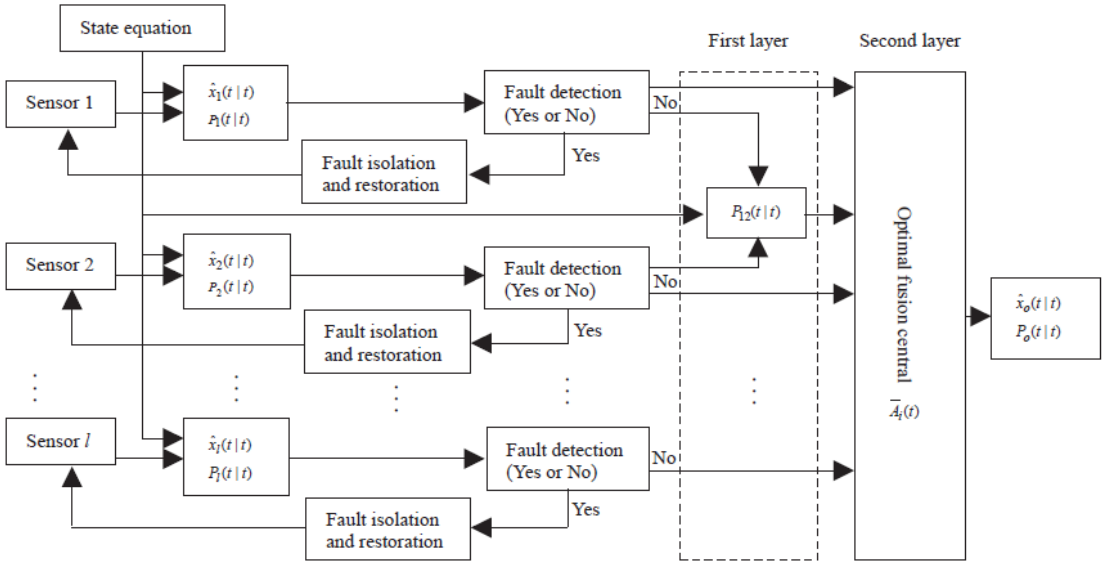

Figure 24: optimum decentralised Kalman filter[23]

The derivation of the fusion algorithm also makes sure that the output states are a better estimator than the sensors separately. The least squared error is smaller.

3.4.2.2 Method I

In the first method, only the velocity is a state in the state space representation. The acceleration is modelled as an input and the noise w depends on the sample frequency. v is the measurement noise of the sensor.

$$\begin{aligned} x_{k+1} &= A * x_k + B * u_k + w \\ z_k &= H * x_k + v \\ With & \\ x_k &= \left[v_k\right], \quad u_k = \left[a_k\right] \\ A &= \left[1\right], \quad B = \left[\Delta t\right] \\ H_{GPS} &= \left[1\right], \quad H_{tachometer} = \left[1\right] \\ w &\sim \Delta t * N(0, Q_k), \qquad v \sim N(0, R_k) \\ Q &= B * B' * \sigma_{acc}^2 = \Delta t^2 \sigma_{acc}^2, \quad R = [\sigma_m^2] \end{aligned} \tag{76}$$

The process noise w_k is assumed to be a zero mean multivariate normal distribution with covariance Q_k. The observation noise v_k is assumed to be zero mean Gaussian white noise with covariance R_k.

3.4.2.3 Method II

There are two states in method II: the acceleration and the velocity. The acceleration is assumed to be Gaussian distributed with mean 0. The advantage of this approach is that the model also works with a faulty acceleration sensor. The disadvantage of this approach is that the process is modelled as a normal distribution with mean 0. In fact that is not the case, but test results will demonstrate if this is a problem.

$$
\begin{aligned}
x_{k+1} &= A * x_k + C * w \\
z_k &= H * x_k + v \\
With& \\
x_k &= \begin{bmatrix} v_k \\ a_k \end{bmatrix},\ A = \begin{bmatrix} 1 & \Delta t \\ 0 & 1 \end{bmatrix},\ C = \begin{bmatrix} \Delta t \\ 1 \end{bmatrix} \\
H_{GPS} &= \begin{bmatrix} 1 & 0 \end{bmatrix},\quad H_{tachometer} = \begin{bmatrix} 1 & 0 \end{bmatrix},\ H_{accelerometer} = \begin{bmatrix} 0 & 1 \end{bmatrix} \\
w &\sim N(0, \sigma_a^2),\ \ v \sim N(0, \sigma_m^2) \\
Q &= C * \sigma_{acc}^2 * C' = \begin{bmatrix} \Delta t^2 & \Delta t \\ \Delta t & 1 \end{bmatrix} * \sigma_{acc}^2, \qquad R = \begin{bmatrix} \sigma_m^2 \end{bmatrix}
\end{aligned}
\tag{77}
$$

Q is not full rank, so it has no probability density function[24]. Another way to simulate this is that $w_k \approx C * N(0, \sigma_a^2)$.

3.4.2.4 Fault Detection

The proposed fault detection method is the weighted sum of residuals(WSSR) method[25] in which the the errors of the last N data points are added with weights dependent on the covariance matrix. The confidence level determines a threshold level. If the WSSR is higher than the threshold, then the sensor is defined as faulty. The challenge is to determine a value for N. A low value of N can result in a lot of sensitivity to small changes in the system. A value of N, which is too large detects a faulty sensor too late. Still there has to be thought about the period in which the sensor is not detected as faulty, where it in fact is. Maybe an extended Kalman filter could be used to estimate the current mean and covariance. If strange values are measured, then the estimate does not change, but the covariance matrix does.

4

Prototype Implementation and Validation Results

After designing the controller and the structure of the program. The hitch force control model was implemented on the E-Connect. This chapter provides a description of the test setup and an analysis of the test results.

4.1 Implementing and Validating the Hitch Force Control Model

The tests of the E-Connect started with testing the CAN-communication. Known sequences were send from one E-Connect to another. This worked, but since the serial UART output could only handle logging 250 messages per second, a higher speed was not tested, this is not a problem since it will only process the brake signal and load cell force, with a total frequency of 160 Hz.
After the communication worked, the system was extended by connecting the hitch connection to the CAN cable and checking if the correct load cell force was transmitted to the E-Connect. The direction of the force was declared opposite to the convention discussed in this report. Therefore, the input force had to be multiplied by -1. The next step was to implement the hitch force control model and to test it without the brakes actually braking. Figure 25 shows the force at the hitch connection during the test. In this test the goal was to test if the controller responded to the load cell force and brake signal. It was also tested if the maximum reference output brake signal is limited. The final step was to include the feedback loop and to test the entire system. The maximum load cell force with an unloaded trailer is 4000 to 5000 N. The unloaded trailer weighted approximately 300 to 400 kg.

Tests showed that the brake force keeps increasing as long as the load cell force is not negative. As soon as the load cell force is negative the brake force will decrease as well. Anti-windup is used to limit both the maximally send brake force as the minimum brake force(zero).

Another test at a higher velocity of 14 m/s resulted in a quickly saturated brake force due to a high braking force of the car. The brake controller current was limited at a certain value for safety reasons. As a result, the trailer could not brake enough and it could be verified if the controller worked.

In the last test the velocity was decreased to 11 m/s and the brakes of the car were applied very slowly so the controller would not reach its saturation point. The result of this test can be seen in figure 26. As can be seen, the load cell force moves around zero N, which is exactly the purpose of the controller. The brake force keeps increasing. That is because the car brakes more heavily at the end. The load cell force swings between + 400 N and -400 N, which is considerably better than the maximum load cell force of approximately 7000N. The trailer was loaded in this test with a water tank of approximately 1000 kg. Therefore, the maximum load cell force without braking would have been higher than visible in figure 26.
Due to the fact that the entire system could be tested for four hours, limited data could be ex-

Figure 25: load cell force of open loop system

tracted. Soon the water tank in the trailer was filled, but that resulted in the current quickly saturating. Next test days should focus at the behaviour of the trailer with a lower mass.

4.1.1 Implementating and Validating the Current Control Model

In preparation for the test days, the current sensor was implemented with the current control model. The current sensor was accurate in measuring DC currents, but not at measuring pulse width modulated currents. The sensor output was dependent on the duty cycle. It was however visible that the current control model worked. If a reference current was entered of 2 A. Then the controller regulated the duty cycle such that the measured current was 2 A. Even though that was not the actual current through the solenoid. It did show that the controller worked correctly. The rise time could not be checked.

4.1.2 Implementing and Validating the Orientation Model Algorithm

The implementation of the orientation model on a microcontroller is out of the scope of this bachelor thesis. However, the simulation is done with actual sensor data. An E-Connect was mounted in a caravan behind a car. A communication cable was wired from the caravan to the car. The information was serially send to the laptop. The simulation is done in Matlab as is shown in section 3.3.2.10. The main problem with testing the algorithm was that the logging of test data was not consequent with the sample frequencies of the different sensors. The amount of samples from the accelerometer were not exactly twice the amount of samples from the gyroscope. During a test of 20 min, approximately 1 second of data was lost. Relatively, that is not a lot, but it makes the orientation model harder to program. A better solution could be that downsampling can be implemented in the controller by averaging x data points and sending with a rate/x. The calibration could be done by first placing the trailer levelled with a spirit level. Moving the jockey wheel upwards made the wheel connected to the jockey wheel move a bit sideways. That disturbs the calibration model. The wheel therefore has to be clamped during the calibration phase.

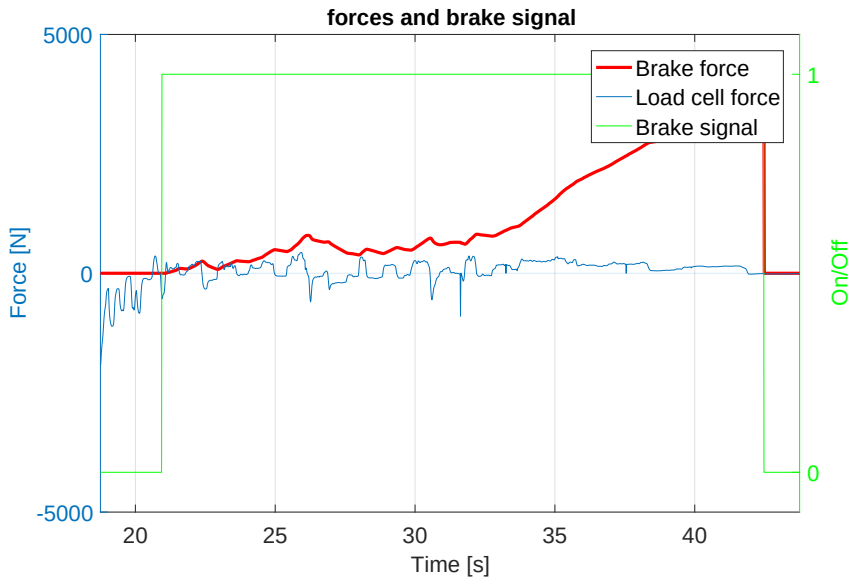

Figure 26: test of whole system at a start velocity of 11 m/s and softly applying the car's brakes, as can be seen the load cell force stays around 0 N.

4.1.3 Implementing and Validating the Sensor Fusion Algorithm

The implementation of the sensor fusion algorithm is out of the scope of this bachelor thesis. The simulation in Matlab was not possible since there was no possibility to log data for the simulation. The reason was that the GPS module from E-Trailer, that communicated via CAN, did not work and only send zeros. The tachometer had a lot of spikes as noise in the data. Reflective material was added at the wheels to detect the turns. There has to be looked into the reflective material used, since the performance just after applying it was better than at a later point of the day.

5

Discussion

The implemented algorithms require sampling of sensor data at specific time points without data loss. At the same time, it is best to make the sample rate as high as possible. That trade-off is clearly visible in the received data. In the orientation model, not all data is received. On a test of 20 minutes, 1 accumulated second of data was lost, which is too much for the evaluation of the gyroscope data. Integrating one second can result in a difference of maximally 20 degrees, which is a lot. If a high pass filter is implemented, then the data loss has less effect. Due to the limited time, no more attention could be spend at the data loss. Different tests with the E-Connect show different drifting properties of the gyroscope. There were tests in which the integrated yaw rate showed angle changes close to 90 degrees. That is very useful for the orientation model. The reason that it was not always the case is because the sample frequency of the microcontroller is not always the programmed sample frequency. A concentration of more important tasks might make the microcontroller skip a sampling point. A solution that was implemented was that a time stamp was added to every send data. Unfortunately, the method was implement too late to do a test with it. The low pass anti-aliasing filter cutoff frequency of the accelerometer was set at 50 Hz. The sampling frequency was 100 Hz. A lot of spikes were visible in the received data. A higher sampling frequency would have been better, since higher frequency signals could be rejected better. It is not possible to lower the anti-aliasing filter cutoff frequency. Therefore, the only solution is to increase the sampling frequency. The question is whether increasing the sampling frequency of the gyroscope helps. The anti-aliasing filter of the gyroscope has a lowest cutoff frequency setting of 12.5 Hz. Sampling with 190 Hz should already be high enough. Tests can be done to check if increasing the sampling frequency helps.

Data from the tachometer showed a lot of incorrect peaks, which should be dealt with in the future. It is also difficult to calibrate the tachometer. We can drive with the trailer 80 km/h and look at the voltage at that point. A linear line can be taken from that point to (0,0). The question is whether the velocity that the car displays is that accurate. A small scale error of the tachometer must be assumed in order to create a good model. Apart from the spikes, the tachometer responds quickly to velocity changes and is a good estimator. During testing, the car sometimes stood still and the load cell force was unequal to zero. As a result, the controller could keep integrating without the load cell force going to zero. Further algorithms should include a statement that makes sure the brake is only activated at speeds higher than 1 m/s. The driver of the car just removed the brake signal after braking as a pragmatic solution. That is not acceptable for the consumer. In order to determine the mass of the car and the trailer, a special force scale for cars was used that was positioned under every wheel separately to determine the weight at that wheel. The weight at the wheel of the trailer was more than the maximum allowed mass of 500 kg. Therefore the weight of the trailer had to be estimated. Next tests should verify the weight with a better scale. Even though the current through the solenoid was often saturated at 4 A, in the car it sometimes felt as if the trailer was braking the car. It was clear that the controller was activated. A faster or slower controller could not directly be identified in the car. The hitch force control model was based on driving in one direction. During the turns, there were no problems with the braking system. Appearantly, the controller works propperly in turns as well.

6

Conclusion

Numerous parties devised requirements for the brake control system. The patent analysis showed that the designed control model is not allowed in the United States and Germany. Still the decision has been made to design the system, because the product will first be introduced in other countries where there are no patents about the electric brake system. The RDW requires the load cell force to be regulated to zero. That part is achieved. It is clearly visible that the load cell force moves around 0N due to the controller. There are deviations, but that is logical as the car driver does not brake constantly and there are disturbances such as wind. The second requirement is that the system responds within 0.6 seconds. The controller has been designed such that it responds within 0.6 seconds. Therefore, that requirement is also achieved. The actual RDW test shown in figure 4 was not done. The tachometer did not provide reliable velocity data to verify the actual test of the RDW. Therefore, the decision was made not to do the classical RDW test, but to test whether the load cell force is properly regulated to zero or not.

The microcontroller has been programmed in a structured manner. The communication via CAN works perfectly and error messages are included in the code. The anti-windup algorithm is successfully implemented and the mailbox system allows the amount of functions connected to the mailboxes to be increased. The advantage of the model based control approach for the hitch force control model is that only one parameter needs to be changed. As a result, the control model can quickly be altered in the program, because only one line of code needs to be changed. The same holds for the current control model. Only the I parameter needs to be changed. The test for the hitch force control model were done without the current control model and showed promising results. The current control model should make the E-Brake even better, since it responds more quickly to temperature effects of the solenoid. Also the temperature effects can be determined.

For problem statement 2, due to safety issues, no data could be collected of the trailer swaying. However, a model is designed that can be implemented with empirical sensor data. The calibration model works accurately. The E-Connect can be mounted in any direction. Both the integrated yaw rate, the yaw rate and the centripetal force can be determined from the gyroscope and the accelerometer. Together with the velocity, swaying can be detected. The next step of problem statement 2 is to determine the dynamic acceleration. The gyroscope is not effective in determining the pitch and the roll. The acceleration sensor could better be used by itself in the current configuration. Still, there has to be looked into the behaviour of the gyroscope, because a correct working gyroscope can have a huge positive impact on the model. The acceleration and deceleration of the car are clearly visible in the predicted Euler angles.

For problem statement 3, a top level decentralised Kalman fusion algorithm is designed with recommendations about fault detection. No conclusions can be drawn about the performance, since there was no data to be logged from the GPS sensor. The basic conclusion is that the designs and implementations of the three problem statements work correctly and can be improved by the changes in the recommendation chapter. The focus of the project, the hitch force control model works correctly.

7

Recommendation and Future Work

Recommendations can be made for the algorithms, testing and software. The current controller and the hitch force control model work correctly with the known masses of the trailer and the car. The next step is to identify whether a robust controller can be created, which does not need the masses to be entered. Attention has to be paid to the fact that there can also be mistakes in the lookup table for example. Without a current control model, also the variations in resistance and inductance of the solenoid need to be taken into consideration. During testing, it was also found that the resistance of the brakes are different per solenoid.

The orientation model and implementation can also be improved considerably. The microcontroller code has to be restructured such that a higher sample frequency of the accelerometer and gyroscope can be used. After that, downsampling can be implemented to send the data at a lower sample rate, while keeping the increased accuracy of a higher frequency. Another interesting feature is to identify the behaviour of the drift for different sensors. The high pass filter can be redesigned as a transfer function of 1 minus a low pass filter. The estimated value of the low pass filter is the drift. In order to determine if the pitch can be measured by a gyroscope, tests have to be done in the mountains at steeper hills. Another part of filter design is phase analysis. Up until now, the phase characteristics were not discussed in the orientation model. For the orientation model to work correctly, there has to be looked to phase delay. It is also possible to measure height differences with a pressure sensor. The pressure sensor could be used in the orientation model to predict the pitch. In that case, also a velocity sensor needs to be incorporated, since the height change also depends on the velocity of the trailer. For the sensor fusion algorithm, the measurement noises can be determined by placing the sensors in the trailer and stand still. The collected data is the measurement noise that can be tested on normality(Jarque Bera) and variance. Next a fault isolation and restoration algorithm needs to be designed for the decentralised Kalman filter. Resetting the sensor can be part of the restoration. Another issue is the sample rate of the sensors. The tachometer has a variable sample rate,the GPS has a relatively low sample rate and the accelerometer has a relatively high sample rate. Filters could be placed after the accelerometer with downsampling afterwards.

Another recommendation for the software part of the future implementation of the E-Brake is to lower the frequency of the timeout timer. The triggered counter is made redundant and decreasing the amount of interrupts which will speed up the system. Another important feature that needs to be implemented is a safety check on the CAN-communication. The brake controllers need to tell the main processing unit when an signal is received. If the received brake force is within the accepted boundaries, then an acknowledge is returned by the brake controller. Another safety measure is to check if the car and the trailer are still connected via the multicon connection on the car, such that the main processor knows if there is a problem in the cable. A solution is to use the load cell force and the accelerometer to determine if the car brakes or not. A deceleration less than 0.4 m/s^2 is seen as the car not braking. Finally it will be a good feature to inform the user of any error by sending a pop-up on its (mobile) dashboard.

References

[1] C. Pasfield, "Electric brake control system for trailers", pat., Australian patent AU2015242938, Oct. 29, 2015. [Online]. Available: http://www.ipaustralia.com.au/applicant/rv-electronics-pty-ltd/patents/AU2015242938/.

[2] J. Diebel, "Representing attitude: Euler angles, unit quaternions, and rotation vectors", *Matrix*, vol. 58, no. 15-16, pp. 1–35, 2006.

[3] *Inertial measurement units ii*, online, May 2017. [Online]. Available: https://stanford.edu/class/ee267/lectures/lecture10.pdf.

[4] *Imu data fusing: Complementary, kalman, and mahony filter*, online, May 2017. [Online]. Available: http://www.olliw.eu/2013/imu-data-fusing/.

[5] F. Caron, E. Duflos, D. Pomorski, and P. Vanheeghe, "Gps/imu data fusion using multisensor kalman filtering: Introduction of contextual aspects", *Information fusion*, vol. 7, no. 2, pp. 221–230, 2006.

[6] Köhler, R. and Kober, K., "Electrical braking device for vehicle trailers and method for operation thereof", pat., US Patent 7,438,368, Oct. 21, 2008. [Online]. Available: https://www.google.ch/patents/US7438368.

[7] R. Köhler and K. Kober, "Elektrische bremseinrichtung für fahrzeuganhänger und verfahren zu deren betätigung", pat., EP Patent 1,448,421. [Online]. Available: https://encrypted.google.com/patents/EP1448421B1?cl=pt.

[8] *Uniform provisions concerning the approval of vehicles of categories m, n and o with regard to braking*, online, Regulations on Braking, Mar. 2014.

[9] *Rolling resistance*, online, unknown. [Online]. Available: http://www.engineeringtoolbox.com/rolling-friction-resistance-d_1303.html.

[10] *Drag coefficients cars*, online, May 2017. [Online]. Available: http://rc.opelgt.org/indexcw.php.

[11] *Automotive aerodynamics: Drag area – size matters*, online, May 2017. [Online]. Available: http://www.curbsideclassic.com/automotive-histories/automotive-aerodynamics-drag-area-size-matters/.

[12] *Aanschaf van een caravan*, online, May 2017. [Online]. Available: http://caravanhandboek.biod.info/ch2-aanschaf.htm.

[13] L. Harnefors and H.-P. Nee, "Model-based current control of ac machines using the internal model control method", *IEEE transactions on industry applications*, vol. 34, no. 1, pp. 133–141, 1998.

[14] G. F. Franklin, J. Powell, and A. Emami-Naeini, *Feedback control of dynamic systems*, fifth. Pearson Education Limited, 2015, ISBN: 1292068906.

[15] *Ultra-compact high-performance ecompass module: 3d accelerometer and 3d magnetometer*, 2013. [Online]. Available: http://www.st.com/content/ccc/resource/technical/document/datasheet/1c/9e/71/05/4e/b7/4d/d1/DM00057547.pdf/files/DM00057547.pdf/jcr:content/translations/en.DM00057547.pdf.

[16] *Inemo inertial module: 3d accelerometer and 3d gyroscope*, 2012. [Online]. Available: http://www.st.com/content/ccc/resource/technical/document/datasheet/bd/61/af/53/b5/f5/4d/7b/DM00037200.pdf/files/DM00037200.pdf/jcr:content/translations/en.DM00037200.pdf.

[17] *Mpu-6000 and mpu-6050 product specification revision 3.4*, 2013. [Online]. Available: https://www.invensense.com/wp-content/uploads/2015/02/MPU-6000-Datasheet1.pdf.

[18] *L3gd20: 3-axis digital output gyroscope*, Feb. 2013. [Online]. Available: https://www.pololu.com/file/0J563/L3GD20.pdf.

[19] *Xtrinsic mag3110 three-axis, digital magnetometer*, 2014. [Online]. Available: http://www.nxp.com/assets/documents/data/en/data-sheets/MAG3110.pdf.

[20] *6-axis sensor with integrated linear accelerometer and magnetometer*, 2017. [Online]. Available: http://www.nxp.com/assets/documents/data/en/data-sheets/FXOS8700CQ.pdf.

[21] *Specifications of approval*, unknown. [Online]. Available: https://cdn.sparkfun.com/datasheets/GPS/GP-20U7.pdf.

[22] *Understanding euler angles*, online, picture of euler angles, 2017. [Online]. Available: http://www.chrobotics.com/library/understanding-euler-angles.

[23] S.-L. Sun and Z.-L. Deng, "Multi-sensor optimal information fusion kalman filter", *Automatica*, vol. 40, no. 6, pp. 1017–1023, 2004.

[24] *The multivariate normal distribution*, online, Jun. 2017. [Online]. Available: http://www.math.uah.edu/stat/special/MultiNormal.html.

[25] Q. Changming and S. Shuli, "Fault detection for systems with missing measurements", in *Control and Decision Conference (CCDC), 2013 25th Chinese*, IEEE, 2013, pp. 1050–1053.